ICARUS 104, 301–323 (1993)

Chronology, Eruption Duration, and Atmospheric Contribution of the Martian Volcano Apollinaris Patera

MARK S. ROBINSON AND PETER J. MOUGINIS-MARK

Planetary Geosciences, Department of Geology and Geophysics, SOEST, University of Hawaii, 2525 Correa Road, Honolulu, Hawaii, 96822

JAMES R. ZIMBELMAN

CEPS National Air and Space Museum, Smithsonian Institution, Washington, D.C. 20560

SHERMAN S. C. WU, KARYN K. ABLIN, AND ANNIE E. HOWINGTON-KRAUS

Astrogeology Branch, U. S. Geological Survey, 2255 North Gemini Drive, Flagstaff, Arizona, 86001

Received February 1, 1993; revised April 26, 1993

Geologic mapping, thermal inertia measurements, and an analysis of the color (visual wavelengths) of the martian volcano Apollinaris Patera indicate the existence of two different surface materials, comprising an early, easily eroded edifice, and a more recent, competent fan on the southern flank. A chronology of six major events that is consistent with the present morphology of the volcano has been identified. We propose that large scale explosive activity occurred during the formation of the main edifice and that the distinctive fan on the southern flank appears to have been formed by lavas of low eruptive rate similar to those that form compound pahoehoe flow fields on Earth. A basal escarpment typically 500 m in relief and morphologically similar to the one surrounding Olympus Mons was produced between the formation of the main edifice and the fan, indicating multistage eruptions over a protracted period of time. Contact relations between the volcanic units and the adjacent chaotic material indicate that formation of the chaotic material occurred over an extended period of time and may be related to the volcanic activity that formed Apollinaris Patera. Stereophotogrammetric measurements permit the volume of the volcano to be estimated at 10^5 km^3. From this volume measurement and an inferred eruption rate (1.5×10^{-2} km^3 yr^{-1}) we estimate the total eruption duration for the main edifice to be $\sim 10^7$ yrs. Plausible estimates of the exsolved volatile content of the parent magma imply that greater than 10^{15} kg of water vapor was released into the atmosphere as a consequence of this activity. This large amount of water vapor as well as other exsolved gases must have had a significant impact on local, and possibly global, climatic conditions.

INTRODUCTION

Rates of eruption and the duration of activity at martian volcanoes are poorly constrained. These issues are relevant to understanding the source regions that feed volcanoes and the effects that eruptions had on the martian atmosphere (Postawko *et al.* 1988, Greeley 1987, Wilson and Mouginis-Mark 1987). Geologic studies of the major martian volcanic constructs show that there are essentially two types: those with extensive lava flows such as Olympus Mons and the Tharsis Montes (Moore *et al.* 1978, Greeley and Spudis 1981, Mouginis-Mark 1981, Zimbelman 1984) and those mostly comprised of pyroclastic deposits such as Hecates Tholus, Tyrrhena Patera, and Hadriaca Patera (Reimers and Komar 1979; Mouginis-Mark *et al.* 1982, Greeley and Crown 1990, Crown and Greeley 1993). However, these previous studies provide few morphologic data for constraining eruption durations. To address the temporal issues of volcanism on Mars, we have identified several morphologic relationships that define the chronology of events that resulted in the present morphology of the volcano. We have then utilized topographic measurements to calculate volumes of erupted material at Apollinaris Patera to constrain rate of eruption and volcano lifespan.

Apollinaris Patera (Fig. 1) is located at the boundary between the northern plains and southern highlands of Mars (9°S, 186°). Unlike the other large martian shield volcanoes, it does not occur in either the Elysium or Tharsis volcanic provinces but is situated in a local basin, bound to the west by a large area of chaotic terrain (Fig. 2). Relative to other martian volcanoes, it is middle aged, possibly forming between major eruptive episodes at the Elysium (older) and Tharsis (younger) provinces. Neukum and Hiller (1981) derived a cumulative crater count for the volcano of 3500–8800 craters >1 km diameter per

0019-1035/93 $5.00

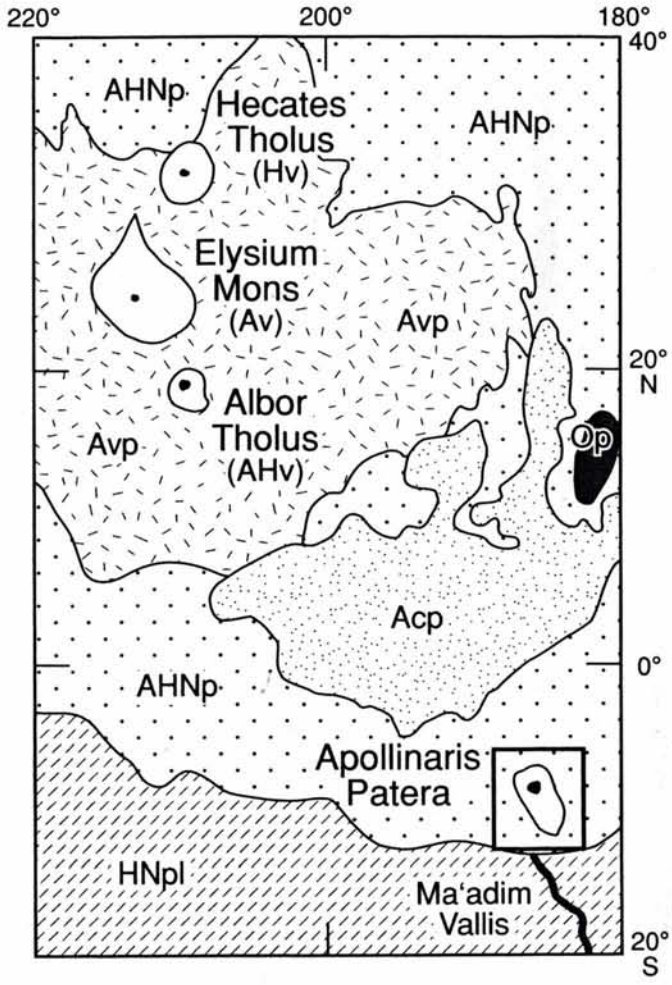

FIG. 1. Generalized geologic map emphasizing Apollinaris Patera and neighboring volcanic features, simplified from Greeley and Guest (1987) and Plescia (1990). Unit designations: Acp, Cerberus plains; AHNp, plains materials; Av, AHv, Hv, volcanic materials; Avp, volcanic plains materials; HNpl, plateau materials; OP, Orcus Patera impact crater materials. Capital letters in unit symbols refer to martian time-stratigraphic periods: A, Amazonian; H, Hesperian; and N, Noachian. The Elysium region is the second largest volcanic province on Mars and contains the three large volcanoes Hecates Tholus, Elysium Mons, and Albor Tholus; it is surrounded by extensive volcanic plains (Avp). Recent mapping by Plescia (1990) and Harmon *et al.* (1992) has identified an extensive area of inferred lava flows north of Apollinaris Patera (Acp). This unit is among the youngest areas on Mars and thus could indicate relatively recent volcanic activity. Apollinaris Patera (heavy box) is located at the major terrain boundary that separates the ancient highlands plateau (HNpl) from the younger lowland plains (AHNp) and is not included in either the Elysium or Tharsis volcanic provinces.

10^6 km^2 (from 635A57; 250 m/pixel), whereas Plescia and Saunders (1979), using different Viking images (088A49,50; 190 m/pixel), derived a cumulative crater count of 990 ± 150 craters >1 km diameter per 10^6 km^2. These values would, respectively, indicate that Apollinaris Patera is Lower Hesperian to Lower Amazonian in age (Tanaka 1986). Attempts to identify an absolute age for the volcano are highly model dependent and give a broad range of absolute ages from 925 ± 140 myr (Soderblom *et al.* 1974) to 3500 ± 15 myr (Neukum and Wise 1976).

Three morphologic features give Apollinaris Patera a distinct appearance (Fig. 2): (1) an unusually large, flat topped summit area (80 km diameter) compared to the E–W diameter (160 km) of the volcano; (2) a large fan of material covering the southern flanks that emanates from a breach in the caldera; and (3) a circumferential basal scarp (West 1974, Scott *et al.* 1978, Plescia and Saunders 1979, Carr and Greeley 1980, Carr 1981, p. 107, Greeley and Spudis 1981, Neukum and Hiller 1981, Basaltic Volcanism Study Project 1981, p. 781, Baker 1982, p. 24, Scott and Dohm in press). Together with a series of flank deposits that suggest early explosive volcanism (discussed below), these attributes illustrate a complex evolution for Apollinaris Patera.

We used radiometrically calibrated and geometrically rectified digital Viking and Mariner 9 images (U.S. Geological Survey 1990), high resolution Viking Infrared Thermal Mapper (IRTM) data, and topographic information derived from stereophotogrammetric analysis of Viking Orbiter images to map and interpret the geology of Apollinaris Patera. The volume of the volcano and the fan material can be determined from the topographic data set, thereby allowing constraints to be placed on the duration of the eruptions and the amount of volatiles that may have been released. In this paper, we present first a morphologic analysis of this intriguing volcano and then speculate on the duration of its eruptions and possible water vapor input to the martian atmosphere.

GEOLOGIC SETTING

Greeley and Guest (1987) mapped the entire volcano as a single unit, AHa (the Apollinaris Patera Formation) at 1 : 15M scale, whereas Scott and Dohm (in press) have recently compiled a 1 : 500K scale map of the region that divides the volcano into four lava flow units. On the basis of surface morphology, thermal inertia values, and color, we divide the flanks into two units that represent different styles of eruption; the main edifice (unit m) and a large fan (unit f) covering the southern flank (Figs. 2 and 4). The fan material is distinct from the rest of the volcano, and indicates a protracted period of activity on Apollinaris Patera (see Fan Materials, below). The nested calderas show that the vent region underwent a complicated sequence of collapse and infilling events. Additionally, formation of the chaotic terrain (unit cht) to the west of the volcano may be related to the formation of the volcano. Finally, we find no convincing evidence that the plains

(unit p) surrounding the volcano is deposits of volcanic materials emanating from Apollinaris Patera and thus agree with the mapping of Greeley and Guest (1987) and Scott and Dohm (in press). This plains unit surrounding Apollinaris Patera is not relevant to our study and will not be discussed further here.

Main Edifice (m)

The primary geomorphologic unit of Apollinaris Patera is defined here as the main edifice (unit m). This unit is heavily modified by valleys, slumps, and superposed impact craters (Figs. 2 and 3). To the east and northeast, the unit extends from the rim of the summit caldera to a basal scarp that generally forms the perimeter of the volcano. The western edge of unit m extends ~15 km beyond the basal scarp. Here the scarp has a subdued appearance due to a relatively thin mantle of younger materials most likely originating as slide deposits from the upper flanks. On the western flank there are scalloped-headed depressions ~5 km across that terminate in hummocky lobes that we interpret to be slumps (Figs. 2 and 4A).

As identified by Gulick and Baker (1990), there are two types of valleys on the flanks of Apollinaris Patera: (1) narrow, incised valleys that generally emanate from the outer caldera and lack tributaries and (2) a valley network on the northeast flank that has short and stubby tributaries (Fig. 2). A few valleys reach the summit on the western flank and appear to have been truncated by caldera collapse as evidenced by their abrupt termination in the caldera scarp and lack of erosion within the caldera itself (Fig. 2). It has been hypothesized that incised valleys on martian volcanoes were formed either through volcanic density current erosion (Reimers and Komar 1979) or by a combination of surface runoff and sapping (Mouginis-Mark *et al.* 1982, 1988, Gulick and Baker 1990). The main criteria used to differentiate between the two processes are that density currents are expected to begin eroding near the summit and are relatively insensitive to local topographic variations (Reimers and Komar 1979), while runoff valleys are expected to exhibit coalescing branches downstream and to be diverted around local topographic obstacles (Fisher 1977, Reimers and Komar 1979, Mouginis-Mark *et al.* 1982). On the basis of these criteria, it seems more likely that the incised valleys on Apollinaris Patera were cut by volcanic density currents. However, we caution that due to the small valley widths (400–1000 m) and moderate resolution of the Viking image data (~190 m/pixel) this interpretation is only tentative. Additionally, it is possible that valleys originally formed by volcanic density currents may be subsequently modified by either runoff or sapping processes (Reimers and Komar 1979, Gulick and Baker 1990).

In addition to the incised channels, the large slumps on the western flank, mentioned above, indicate that flank material (m) is easily eroded and degraded, analogous to materials that compose many slumps on the Earth (Bloom 1978, p. 178). This friable nature is consistent with an interpretation that the main flanks (m) are composed of a significant amount of poorly consolidated pyroclastic material (see Discussion).

Outer Caldera (cf1)

The outer caldera floor is relatively rough, with portions sloping into the smoother, flat-floored inner caldera (cf2). To the west the bounding scarp of this unit (cf1) appears to truncate flank (m) valleys, and no valleys occur within the caldera, indicating that valley formation occurred prior to formation of the outer caldera (cf1). The raised rim that defines the outer margin of this unit is interpreted to be a scarp related to an earlier caldera, which was partially infilled by later activity, resulting in the general flat-topped nature of the volcano. The inward slope of the floor in the southeast portion (1-3°—see Volcano Topography, below) indicates that substantial subsidence occurred subsequent to the caldera infilling eruptions that formed the inner caldera floor (cf2); the sloping floor is easily seen in Fig. 4A. We note that no flow lobes or wrinkle ridges are visible within the floor materials (cf1) with the currently available images that would further support an origin through effusive lava.

Chaotic Material (cht)

Unit cht is characterized by distinct elevated knobs west of the volcano, typically 1 to 10 km across, that occur in groups and as isolated mesas (Figs. 2 and 3). The margin of this unit and the surrounding plains unit (p) is not distinct but rather transitional, and no conclusive embayment relations are evident. This unit roughly corresponds to the Hcht (chaotic material unit) of Greeley and Guest (1987) and Scott and Dohm (in press), which are interpreted to be erosional remnants of a heavily modified preexisting terrain. Chaotic material, or terrain, is generally accepted to be the result of removal of large volumes of ground ice from within the interstices of the original frozen ground (Sharp 1973; Carr and Schaber 1977). The contact between the chaotic material (cht) and the western flanks (m) of Apollinaris Patera indicate that this process continued after the main edifice building eruptions as the lower western flank is chaotically disrupted (Figs. 3 and 4B). This observation is important because it establishes that significant amounts of groundwater/ice existed around Apollinaris Patera during the main eruptive phases. Additionally, materials that we interpret to be associated with the formation of the fan (f) overlie the

FIG. 2. (A) Image map of Apollinaris Patera, showing the flat-topped summit area, the fan material, the basal scarp, and slump blocks (see B for locations of features). Digital mosaic in sinusoidal equal-area projection with a resolution of ~190 m/pixel; from Viking orbit 088A, width of image is ~235 km, north is to the top. (B) Sketch map of the main physiographic units under study. Unit **m** is the main edifice, unit **cf1** is the outer caldera, unit **f** is the fan material, and **cf2** is the inner caldera all of which compose the volcanic products of Apollinaris Patera. Unit **cht** is a broad area of chaotic terrain that is generally believed to be the result of the removal of large amounts of ground water/ice (Sharp 1973, Carr and Schaber 1977, Greeley and Guest 1987). Note that the chaotic terrain (**cht**) includes disrupted material of Apollinaris Patera which is not mapped separately for the purposes of this work. The undivided plains unit **p** is simplified from Guest and Greeley (1987) and is not directly related to any identifiable volcanic activity from the Apollinaris Patera. The distinct basal scarp is indicated by the triangles.

boundary scarp between the main edifice and the chaotic materials (see Figs. 3 and 4) in agreement with Scott and Dohm (in press). From the existing relations it is not possible to resolve whether chaotic material existed before the activity that built the main edifice (m). On the basis of these contact relations the formation of at least

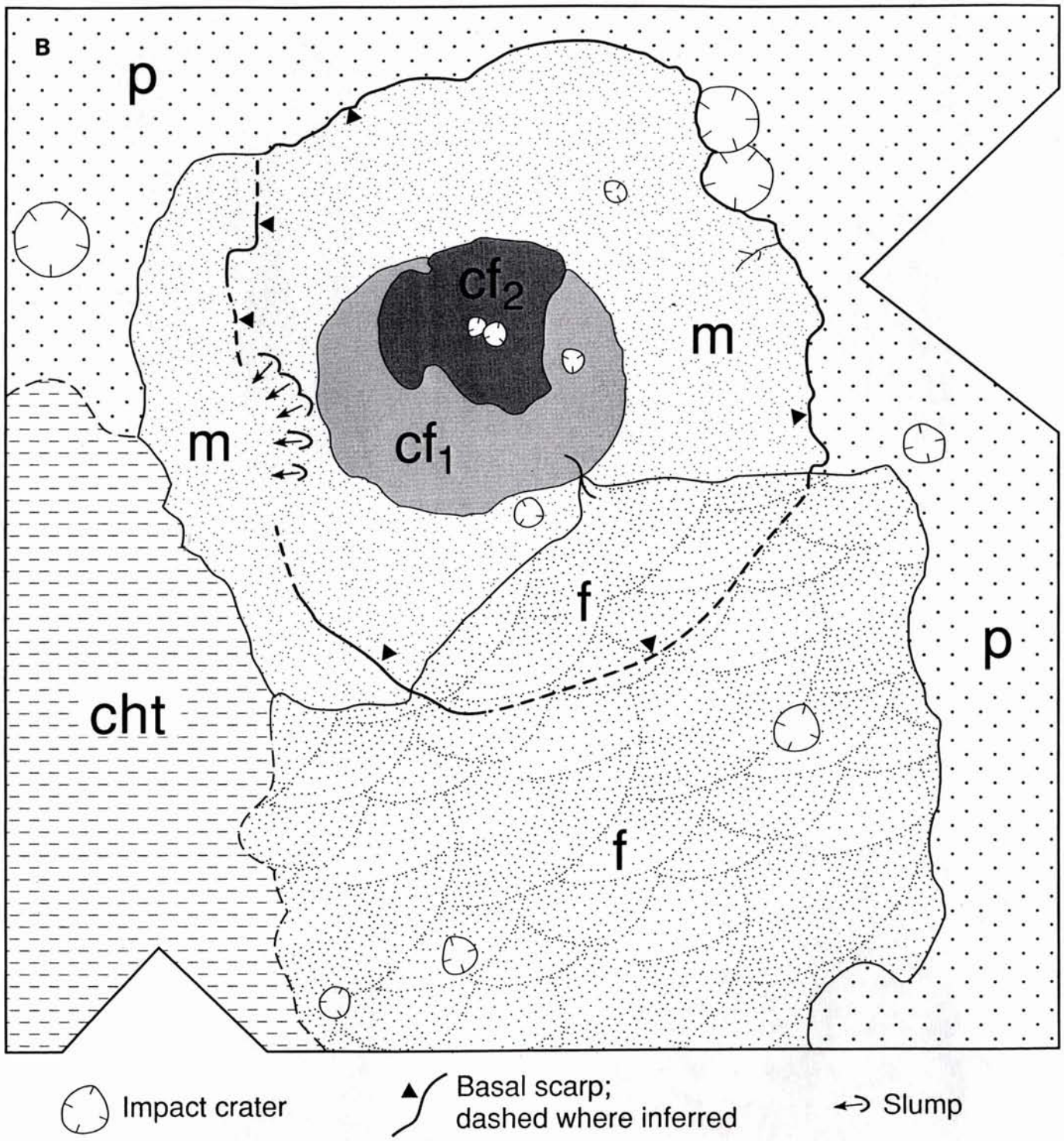

FIG. 2–*Continued*

some of the chaotic terrain must have occurred during the lifetime of the volcano; before and after the emplacement of the fan. This suggests that chaos formation took place over an extended period of time, possibly on the order of millions of years, and may have been due to an increased geothermal gradient from the volcano. This contemporaneous activity with the volcano has important implications for the style of eruption and climatic conditions that may have prevailed during the eruptive phases of Apollinaris Patera (see Discussion, below).

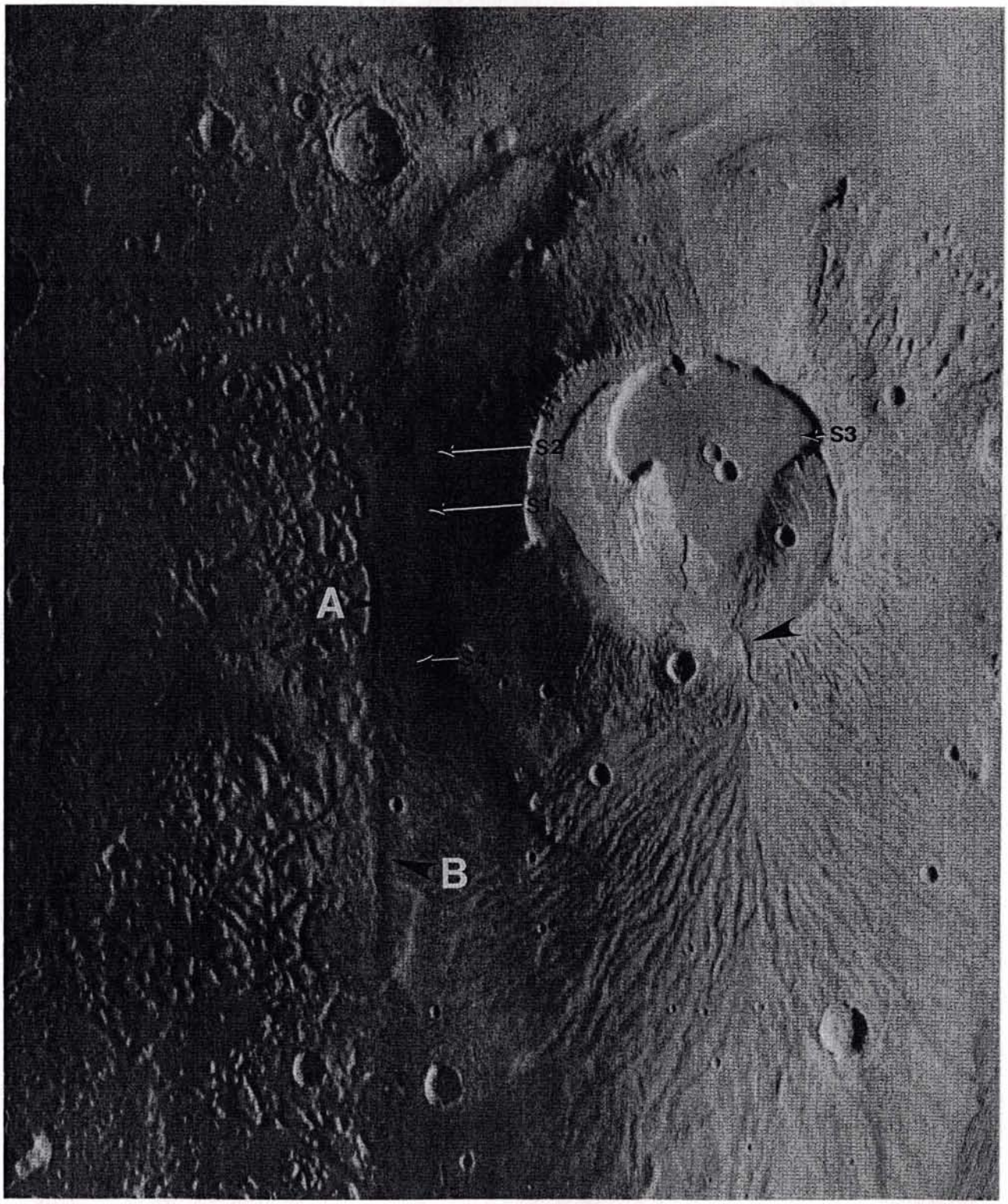

FIG. 3. This large incidence angle image of Apollinaris Patera shows the structure of the fan material and the breach in the caldera wall (unlabeled large arrow). Arrowhead labeled A indicates location where chaotic disruption of the main flank (m) material has occurred, while the arrowhead labeled B shows where fan materials (f) have covered chaotic material (cht). Note lack of incised valleys within the caldera; this is particularly significant on the eastern side of the caldera where interior slopes are comparable to exterior slopes that do have incised valleys (see text). The arrowed locations marked with Sx indicate shadow measurements: S1 = 4800 m, S2 = 4600 m, S3 = 800 m, S4 = 2100 m (all measurements ±100 m). Viking Orbiter frame 635A57, INA = 80°, width of image is ~235 km, north is to the top.

FIG. 4. (A) Perspective view of Apollinaris Patera as seen from the NW looking across to the SE, vertical exaggeration 2×. Of particular interest are the slump blocks on the western flank and the embayment relation between the inner caldera (cf2) and the outer caldera (cf1). Image was created from Viking digital mosaic of images from orbit 088A (see Fig. 2) and topographic data derived in this study. (B) Perspective view showing the distinct fan on the southern flanks of Apollinaris Patera as viewed from SW of the volcano, vertical exaggeration 2×. The arrowhead labeled A indicates region where chaotic material was formed after emplacement of volcanic materials. The label B indicates region where fan materials overlie chaotic materials. Unlabeled arrow indicates breach in caldera from which fan materials appear to have emanated. Image was created from Viking digital mosaic of images from orbit 088A and topographic data derived in this study.

Fan Materials (f)

A large fan extends down the southern flank of Apollinaris Patera for more than 150 km from the rim of the caldera, giving the volcano its distinctive asymmetrical shape (Figs. 2, 3, and 4). The apex of the fan coincides with a channel that breached the south caldera rim (Fig. 3), through which the fan material appears to have flowed, covering the basal scarp and spilling across the surrounding plains (Plescia and Saunders 1979, Carr 1981, p. 107, Neukum and Hiller 1981, Scott and Dohm in press). This channel cuts the outer caldera floor (cf1) and our topographic data show that the channel within the caldera slopes toward the caldera interior. If this channel was indeed formed by the materials that compose the fan, then substantial subsidence of the caldera occurred after fan formation and prior to emplacement of inner caldera materials (cf2—see Inner Caldera, below); thus the inner

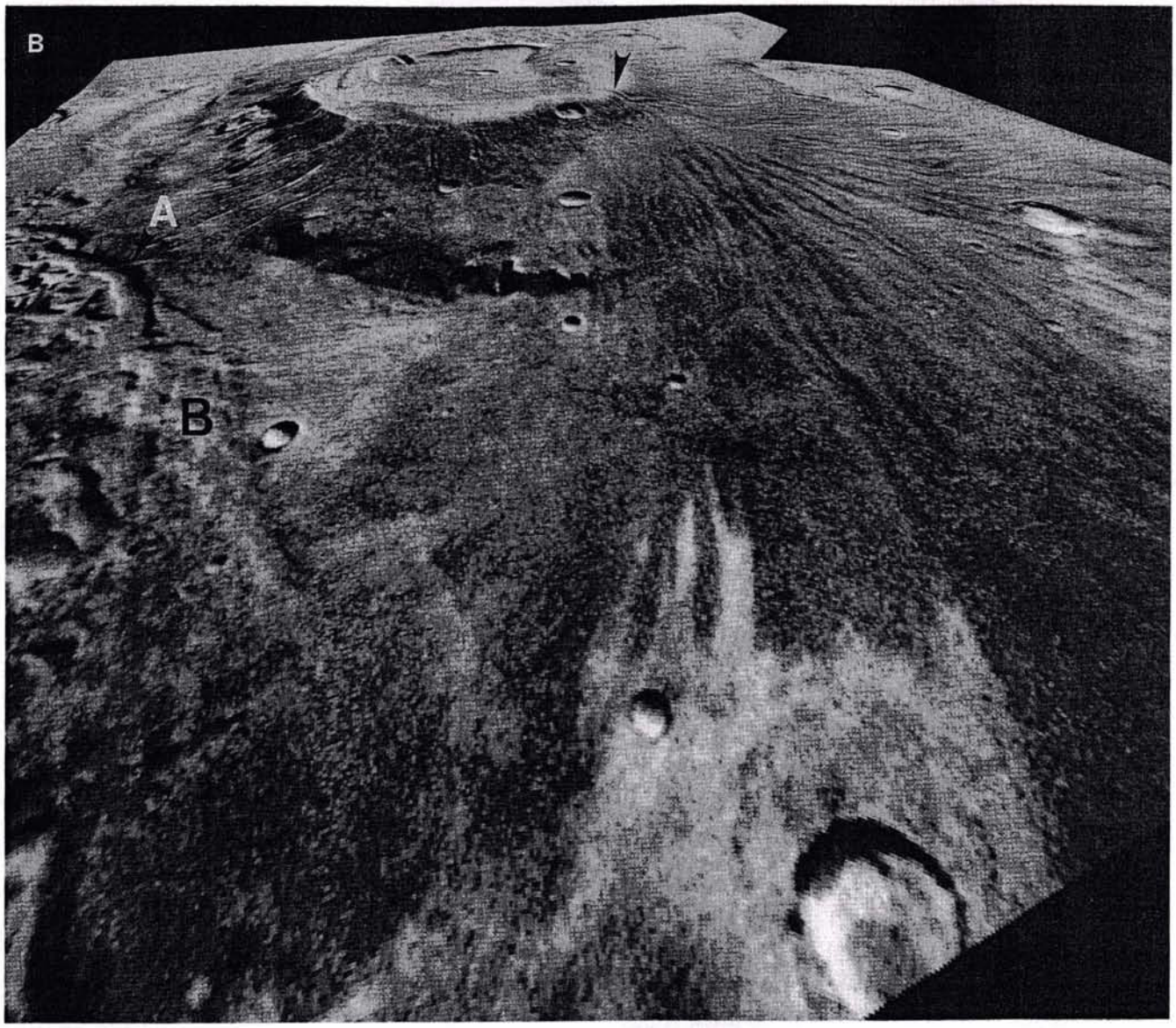

FIG. 4–*Continued*

caldera materials (cf2) are apparently younger than the emplacement of the fan deposits.

The eastern margin of the fan is embayed by the surrounding plains and therefore predates the last episode of plains formation (Scott and Dohm in press). The western part of the fan drapes the bounding scarp between the adjacent chaotic material and the main edifice, and infills low areas between hummocks. This results in the relatively subdued morphology observed in the chaotic terrain in this area (Figs. 3 and 4B). The contact between the fan and the main edifice is sharp, with the fan draped over the basal scarp and the preexisting valleys. Therefore, the fan is younger than the main edifice. We estimate that the material that composes the fan is relatively thin (100–250 m) based on the observation that the preexisting topography of the underlying basal scarp is still evident both in the images and in our topographic data (see Volcano Topography, below).

Several morphologic features suggest that the fan consists of material that is significantly different from the main edifice unit (Figs. 2, 3, and 4B). We note that the fan is not cut by the distinctive, sharply incised valleys that are common on the main edifice. Valleys on the fan are typically wider than those on the edifice; 2–4 km vs

200–1000 m, respectively. Examination of digital pixel values shows that the valley walls on the fan do not cast pixel sized shadows in images with the sun ~12° above the horizon (the valley walls on the main flanks cast shadows), and thus they have relatively shallow-sloping walls. It is not clear whether these valleys are erosional or just low areas between constructional features. We interpret that the fan is mostly composed of effusive materials and this will be discussed below (see Discussion, below).

Inner Caldera (cf2)

The relatively smooth floor of the inner caldera (cf2) embays the sloping margins of the outer caldera materials (cf1) and is thus the younger of the two caldera units. The distinct scarp that forms most of the boundary of this unit ranges in height from about 800 to 1500 m (see Volcano Topography, below). The boundary scarp to the north and northeast cuts across the outer margin of the previous summit-defining caldera (cf1), resulting in an outer rim elevation that is relatively low (4500 m vs 5000–6000 m). This relation is particularly important as it indicates that any effusive activity that we hypothesize to have formed the fan (see Discussion, below) could not have emanated from within the summit after the formation of the inner caldera (cf2); flowing material would have escaped the summit region to the north at this low point (see Volcano Topography, below). This geometry indicates a complex tectonic history which maybe similar to the evolution of other calderas on Mars, such as those at Olympus Mons (Mouginis-Mark and Robinson 1992) and Ascraeus Mons (Zimbelman and Edgett 1992). We note that none of these steep scarps are incised by valleys like those on the outer flanks (unit m) possibly indicating a more competent material. In agreement with Scott and Dohm (*in press*) we infer that the flat, smooth floor of the inner caldera was formed as a lava pond, thus implying that effusive activity dominated final eruptive activity at the summit. However, we note that no flow lobes or wrinkle ridges that would further support this interpretation are visible with the currently available images.

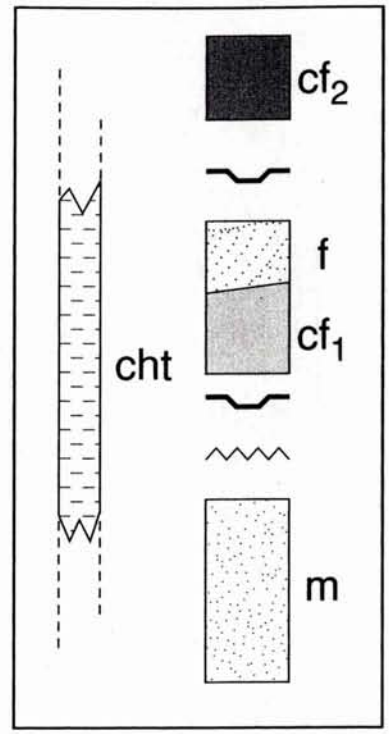

FIG. 5. Stratigraphic column showing the chronology of events that have resulted in the present morphology of Apollinaris Patera (see Fig. 2 for location of units). Initially the main edifice (m) was emplaced, then basal scarp and valley formation (jagged line) occurred. Next, outer caldera formation (broken line) with subsequent infilling (cf1), fan (f) emplacement, possibly as a result of late stage overflow from cf1 deposits, and finally inner caldera formation (broken line) with infilling by ponded lava deposits (cf2). Formation of chaotic terrain (cht) adjacent to the volcano both preceded and followed emplacement of the fan materials.

CHRONOLOGY SUMMARY

Based on the mapping and data analyses presented above we can set forth a chronology of six major events that have resulted in the present morphology of the volcano (Fig. 5): (1) emplacement of the main edifice (m) through mostly explosive activity, (2) formation of the basal scarp, (3) erosion of valleys on the main flanks (f), (4) formation of the outer caldera (cf1), (5) emplacement of the fan materials (f) through effusive activity, and finally (6) formation of the inner caldera (cf2), including effusive lava that ponded to form the present floor. These events are not necessarily temporally distinct, but are gradational in some cases. For instance, basal scarp formation may have commenced during the latter part of event 1, and eruption of the materials comprising the fan may be related to late stage intracaldera activity of stage 4. Formation of the adjacent chaotic material appears to have occurred throughout much of the lifetime of the volcano, thus indicating that this process is long lived.

PHYSICAL PROPERTIES OF THE VOLCANO

To aid in our interpretation of the morphologically defined volcanic units we examine Viking Infrared Thermal Mapper (IRTM) data and Viking color image data. These data are examined to identify any gross physical properties that may be used to show convincingly that the fan and main edifice are indeed separate geologic units.

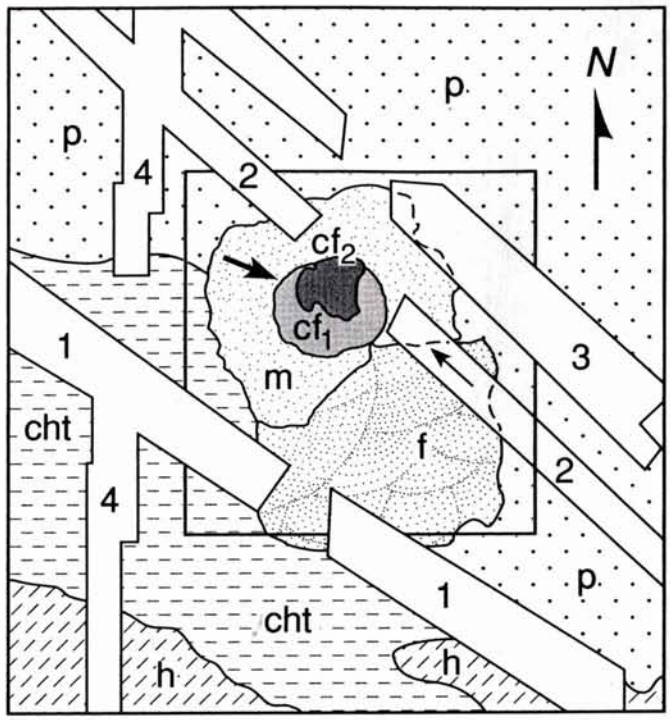

FIG. 6. Schematic diagram showing IRTM data passes near Apollinaris Patera: (1) A569-7, (2) A648-2, (3) A492-8, (4) B551-11 (letter corresponds to Viking Orbiter, three digit number orbit designation, and one or two digit number is the sequence within particular orbit). Dashed lines within IRTM swaths indicate thermal inertia (I) boundaries that correspond with mappable geologic units. Of special interest to this study is the small (ΔI = 0.5) but distinct thermal inertia boundary between the fan (f) and the main edifice (m) indicated by dashed line (small arrow) within data pass 2. Large arrow indicates viewpoint for Fig. 7 that illustrates the sharpness of this boundary. The data tracks that do not cross the volcano were included to check the calibration where data overlapped; we observed no systematic calibration problems in these areas. Solid box shows area covered by Fig. 2.

Thermal Inertia

Two high resolution IRTM data passes cross Apollinaris Patera (Fig. 6). Thermal inertia (I) is derived to estimate the effective grain size of materials on the martian surface (Kieffer *et al.* 1977, Zimbelman and Leshin 1987). The IRTM data were processed to $\frac{1}{8}°$ bins following the procedure outlined by Zimbelman and Leshin (1987). Using the standard Viking model (Kieffer *et al.* 1977) thermal inertia (I) values are derived and are reported in units of 10^{-3} cal cm^{-2} s$^{-1/2}$ K^{-1}. The thermal inertial values are used to test our hypothesis that the flanks and fan materials on Apollinaris Patera are separate geologic units.

A spatial uncertainty in the location of the highest resolution IRTM tracks on the surface occurs due to gravitational perturbations of the spacecraft orbit near periapsis (Zimbelman and Leshin 1987). To correct for this positional offset, we manually shifted IRTM orbits by matching high frequency thermal inertia signatures with the locations of impact craters and discrete low albedo patches that are easily identified in both data sets. To compensate for any temperature shifts in the data caused by minor atmospheric effects from dust and clouds, we compared relatively bland regions in our high resolution IRTM data with known thermal inertia values from the Mars Consortium digital thermal inertia map (Kieffer *et al.* 1981) to derive an offset. The thermal inertia values in respective orbits agree at intersection points lending a high degree of confidence to the accuracy of the correction procedure (Fig. 6). We also applied an elevation correction to compensate for atmospheric pressure effects on the surface thermal conductivity (Zimbelman and Greeley 1983) using the Mars Consortium global topographic data (Kieffer *et al.* 1981). The errors associated with these elevation data are reported to be on the order of 1 to 2 km. Elevation effects are sensitive on the order of a scale height (10 km) which leads to a change of about one thermal inertia unit or less, dependent on the magnitude of the thermal inertia value (Zimbelman and Greeley 1983); therefore, the generalized topography can be used to produce a first-order correction. Comparison of temperatures derived from four IRTM wavelengths (7, 9, 11, 20 μm) confirms that the anomalies reported here are not artifacts of atmospheric contamination (Christensen and Zurek 1984).

Our derived thermal inertia values exhibit anomalies that can be directly correlated with geomorphic features other than albedo patterns. We find a one-to-one correspondence between the distinct morphologic and thermal property boundaries. Figure 6 shows a map with the location of IRTM data passes in relation to our mapped units; on this figure the correspondence of the thermal inertia boundaries and geologic boundaries is apparent. Such a strong correlation is unusual for Mars, based on previous work examining martian volcanoes (Kieffer *et al.* 1977, Zimbelman and Kieffer 1979, Zimbelman and Leshin 1987). A thermal inertia transition exists that corresponds to the boundary between the main edifice (I = 3.8 to 4.5) and the surrounding plains (3.0–3.5), which agrees with previous work (Crown *et al.* 1988). Of greater importance to the interpretation of the volcano, we find an intravolcano thermal inertia anomaly (of intensity 0.5 thermal inertia units) between the fan (I = 4.4, number of samples = 9) and the main edifice (I = 3.9, number of samples = 9; see Figs. 6 and 7). This boundary cuts across topographic contours, and thus we dismiss the possibility that it is simply due to elevation effects.

Previous work examining volcanic deposits on Mars using IRTM data indicates that it is difficult to assign a specific thermal inertia value to a geologic unit, mostly due to the complications arising from variable dust mantling

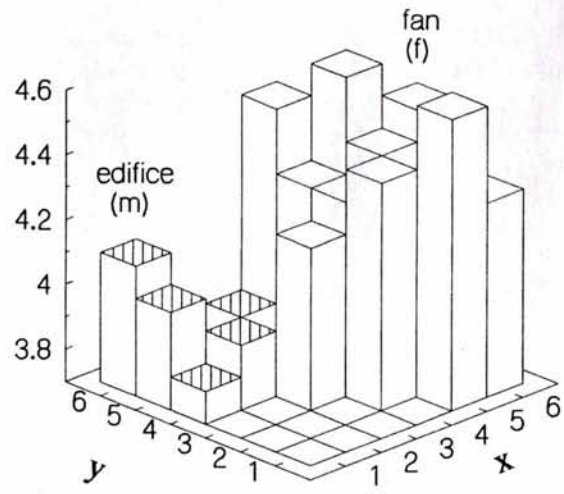

FIG. 7. Three-dimensional plot of IRTM thermal inertia values for the edifice (m; hatchured samples) and fan (f), showing the distinct thermal inertia boundary between these two units (see text). The x and y axes show relative position within IRTM track A648-2, each sample is approximately $\frac{1}{8}°$ (7.5 km). The z, or vertical axis, shows thermal inertia (I). This perspective is looking from the NW to SE (see arrow in Fig. 6 for viewpoint) at the contact between the fan and the main edifice shown as a dashed line (small arrow) within track 2 of Fig. 6.

(Zimbelman 1984). For a given rock type, the thermal inertia value can range dramatically, depending on the amount of exposed bedrock, thickness of dust mantle, and grain size of the dust. For example, Mouginis-Mark *et al.* (1988) have identified possible pyroclastic deposits on Alba Patera that have thermal inertia values between 1 and 4, whereas Crown *et al.* (1988) found that materials at Hadriaca Patera interpreted to be of pyroclastic origin have thermal inertia values ranging from 5 to 9. Therefore, it is not possible to interpret a thermal inertia value alone as an indicator of a specific geologic material. Nevertheless, in the case of Apollinaris Patera, the underlying rock units have a detectable effect on the thermal signature. Specifically, this difference in thermal inertia between the fan and the main edifice is most likely due to an increased "effective" grain size of the materials composing the fan relative to the main edifice. This most likely is the result of a difference in the proportion of eolian component to rock abundance on the surface or an actual change in grain size of the eolian component (see Color, below), not the result of a change in mineralogy of the bedrock. In the case of the units identified on Apollinaris Patera the fan (f) may have a more blocky structure than the main edifice (m) resulting in a slightly higher rock abundance and a correspondingly higher I.

Color

The relative color variations of the martian surface are grossly controlled by the particle size distribution of the pervasive eolian dust cover that mantles the planet (Arvidson *et al.* 1989, Herkenhoff and Murray 1990, Soderblom 1992). With a coarser eolian component the surface exhibits a darker albedo and "bluer" visible color. Previous analyses comparing albedo (which is often directly related to color) and thermal inertia indicate that eolian component particle size strongly controls the thermal inertia of the surface (Kieffer *et al.* 1977, Zimbelman and Kieffer 1979, Keiffer *et al.* 1981, Soderblom 1992). The distinct thermal inertia boundary within Apollinaris Patera identified here has no diagnostic spectral signature within the visible bandpasses of the Viking Imaging system (orbits 506A, 609A, 468S). This was checked by examining color ratios (red/violet) of these three color orbits (Table I) to

TABLE I
Mariner 9 and Viking Orbiter Images of Apollinaris Patera, Mars, Including Pertinent Acquisition Parameters

Orbit	EMA	INC	PHA	FIL	Ls	RES	AZ
177A13[a]	01	38	38	mB	243	1000	270
088A50	44	38	82	C	123	192	047
506A75	09	38	39	VGR	359	585	280
603A42	29	69	47	R	46	614	062
609A47	26	27	28	VCGR	48	835	002
635A57	23	79	94	R	59	250	069
639A92	19	45	55	R	61	720	044
646A41	30	78	47	R	64	800	066
687A18	21	54	55	VCGR	82	700	058
806A09[b]	60	65	75	R	137	800	070
372S56	42	48	83	R	86	233	306
468S19	35	39	69	VBGRCmB	131	535	045

Note. For orbits with color data, only the red frame number is listed. EMA, emission angle; INC, incidence angle; PHA, phase angle; FIL, filter (V, violet; B, blue; G, green; R, red; C, clear; mB, minus blue); Ls, aerocentric longitude; RES, resolution in m/pixel; AZ, sun azimuth.

[a] Mariner 9 image.

[b] exact viewing geometry not known, parameters estimated and subject to large error (± 10°).

determine if color boundaries coincide with the morphologic/thermal inertia boundary. Since we found no correlation, we interpret that the eolian component that dominates the optical surface is relatively homogeneous. That is, there is no gross change in particle size of the fine component (that would show up as a color anomaly) while near surface thermal properties are heterogeneous, implying that the surface of the fan (f) is relatively blocky; the physical properties of the underlying materials have a small yet significant influence on the derived thermal inertia. Specifically, we interpret this to indicate an increased rock component due to a relatively rough lava surface of the fan (m). The main edifice (m) which we interpret to be composed of pyroclastic deposits has a relatively smoother surface with a greater percentage being covered with dust (less rocky).

VOLCANO TOPOGRAPHY

Important to our study of Apollinaris Patera are new high resolution topographic data derived through shadow measurements and stereophotogrammetric mapping. These data allow us to establish accurately the volumes of erupted products at Apollinaris Patera as well as to define the overall third dimension of the volcano, and thus aid in constraining its evolution. We derived these new data because the existing published topographic data for Mars (1 : 15M) have an estimated accuracy of 1000 to 1500 m at best (U.S. Geological Survey 1989); for the section of this map covering most of Apollinaris Patera no stereo measurements had previously been made. Our new measurements allow constraint of the topography to a high degree of precision and accuracy, as high as ±100 m in local areas and ~800 m overall. Additionally, these data have been used to update the U.S. Geological Survey 1 : 2M topographic map of the Aeolis Quadrangle which covers Apollinaris Patera (U.S. Geological Survey 1991).

Shadow measurements taken from calibrated digital image data can be very precise under the following conditions; (1) sun angle above the horizon is low, and (2) pixel size is much smaller than the feature being measured (Arthur 1978). These conditions are met by Viking frames 635A57 and 646A41 (see Table I) for the area that contains Apollinaris Patera. Our shadow measurements (see Fig. 3) were taken to provide local, highly accurate, spot measurements to aid in our interpretations, and as a check on the accuracy of our stereo measurements. We estimate the accuracy of the shadow measurements based on the assumption that the top and bottom of the shadow can each be determined to within 1 pixel (total error, E, of 2 pixels) by:

$$E = \sin(90° - \text{INA})\ (2 \times (\text{pixel width})),$$

where INA is the local solar incidence angle and pixel width is the resolution of the image data.

To give lower limits on the total relief of Apollinaris Patera several shadow measurements were taken on the western flanks from image 635A57 (250 m/pixel; Fig. 3). These measurements indicate a minimum relief of 5100 ± 100 m, which is significantly greater than the total relief shown on the U.S. Geological Survey 1 : 15M map (U.S. Geological Survey 1989), 4000 ± 1000 m. This shadow measurement is considered a minimum because any relief upslope from the top of the shadow and downslope from the bottom of the shadow is not included. From the same low sun angle frame we also measured the height of the east rim of the caldera to be 770 ± 100 m. Where possible we checked these measurements with those from 646A41 (800 m/pixel) and found consistent results. In all cases the shadow measurements and stereophotogrammetric measurements matched within the limits of the methods (see Appendix).

Viking Orbiter images can also be used to derive stereophotogrammetric data if favorable viewing geometry exists between overlapping images (Arthur 1977, Wu *et al.* 1982). This method has been used extensively to compile a global topographic data set at moderate resolution (± 1–2 km; Wu *et al.* 1985, 1988) and to acquire local, high resolution topographic contours (Wu *et al.* 1984) and profiles (Blasius and Cutts 1981, Robinson and Tanaka 1990). For this study we selected a pair of Viking images that has a very strong base-to-height ratio (B/H; see Wu *et al.* 1982) resulting in strong parallax and thus accurate topographic measurements (Viking images 603A42 and 639A92—B/H = 1.04). An analytical stereoplotter was used to collect the stereo measurements. The topographic data were acquired in both profiling and contouring modes (see Appendix and Figs. 8–10). The profiling mode results in a more precise measurement than the contouring mode, but is limited in its areal coverage. Therefore we selected specific profiles to address directly pertinent scientific issues (Fig. 8). The contour data are used in a more general sense to provide synoptic coverage for the volcano and surrounding area and were used to update the MC 23NE 1 : 2M topographic map (U.S. Geological Survey 1991).

The elevation data were collected for the 1 : 2M scale contour map with a contour interval of 1 km (Fig. 10). We estimate the horizontal accuracy to be 1000 m and the vertical accuracy to be 800 m relative to the Mars control network. The vertical accuracy of these measurements may be as high as 300 m within the stereo model (see Appendix). For our purposes we converted the contour map to a raster-based digital elevation model (DEM) by first digitizing the contours and then interpolating to a continuous surface (U.S. Geological Survey 1990). This process allowed the volume of the volcano to be calcu-

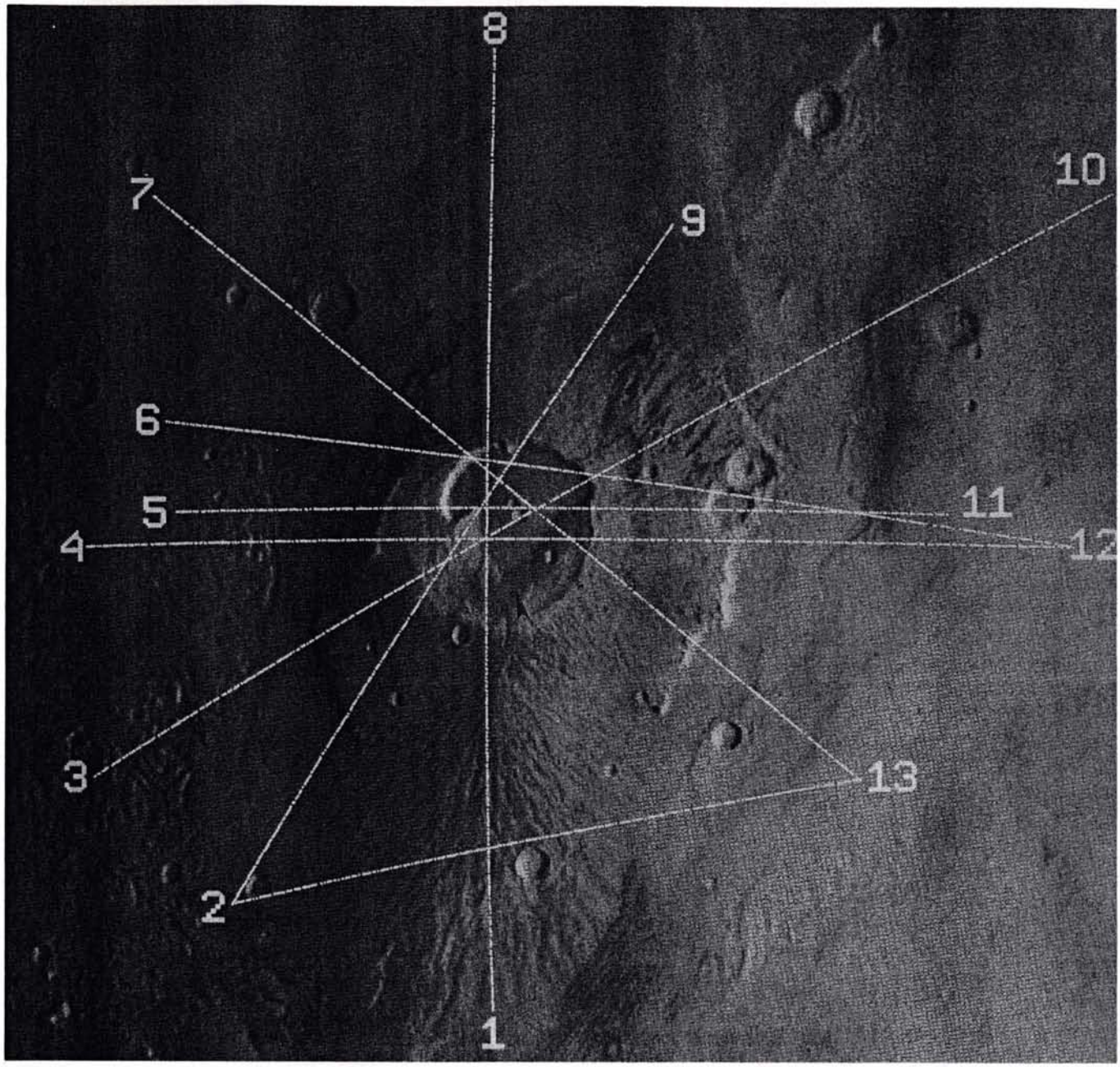

FIG. 8. Location of stereophotogrammetrically derived elevation profiles that cover the major features under study at Apollinaris Patera. Arrowhead denotes downslope direction of caldera floor containing the source channel for the fan materials (see Fig. 9). Numbers identify beginning and ending points for profiles. Profile 4–12 is approximately 400 km in length; Viking frame 603A42.

lated and was also used as a base for creating point perspective views of the volcano (Fig. 4).

From these newly derived topographic data, we determine the volume of Apollinaris Patera (both the main edifice and the fan) to be ~100,000 km^3. An ambiguity arises in this calculation due to uncertainty regarding the actual base of the volcano relative to the preexisting topography. We bracketed our estimate by using the 100 m and the 750 m elevations, which generally correspond to the lower and upper portions of the basal scarp, respectively. The resulting volumes are 103,000 km^3 and 97,000 km^3; therefore we report the volume of Apollinaris Patera to be ~100,000 km^3.

In order to assess the relative significance of the deposits that compose the fan, we estimate its volume separately from that of the rest of the volcano. To do this we

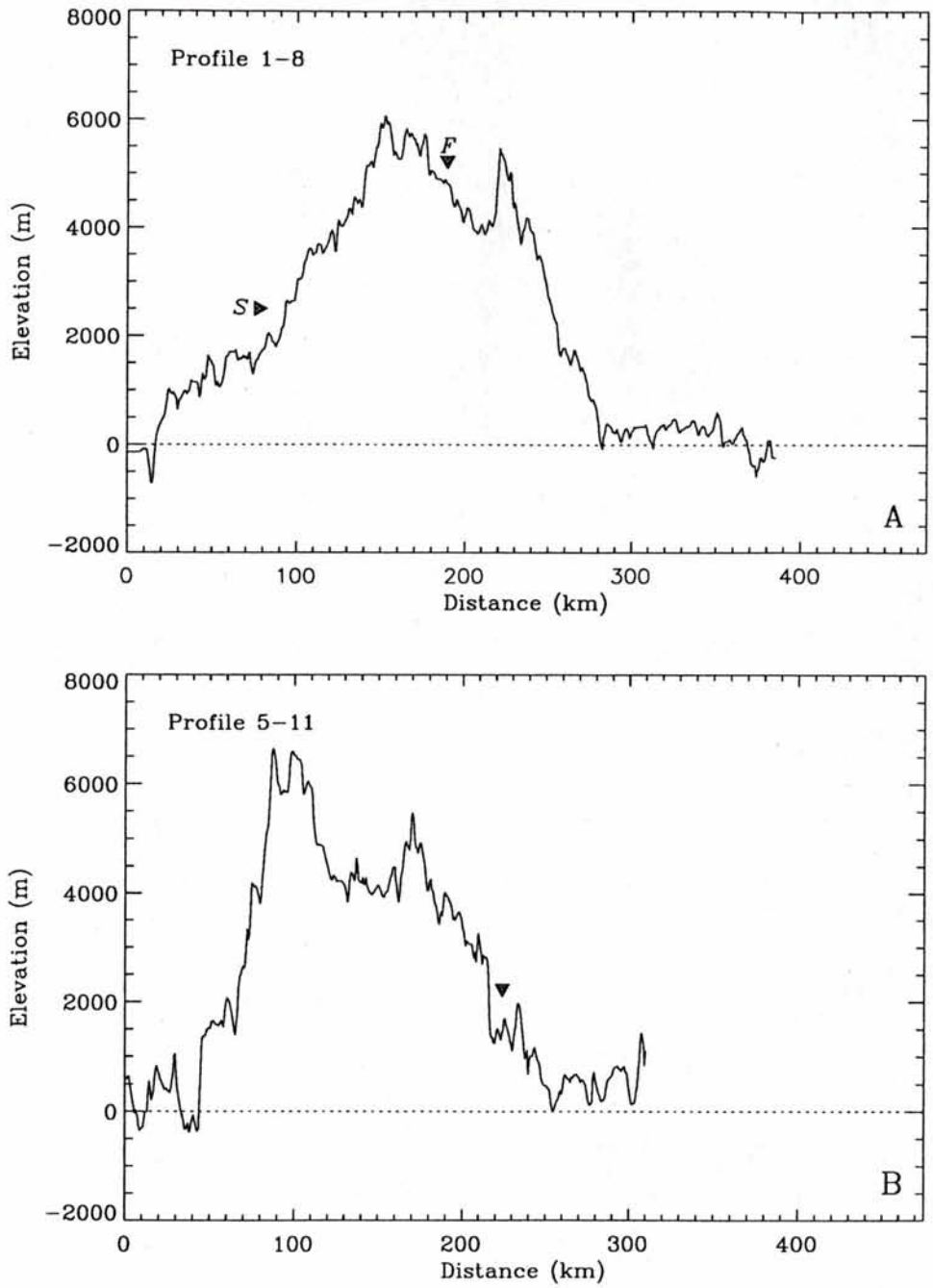

FIG. 9. (A) Stereophotogrammetrically derived topographic profile (Profile 1–8; see Fig. 8 for location) across the volcano from south to north. Horizontal triangle (labeled *S*) indicates the topographic expression of the basal scarp beneath the fan materials, while vertical triangle (labeled *F*) locates inward sloping surface of the outer caldera floor (cf1) which contains the putative source channel for the fan materials (f). The dotted line indicates the zero elevation contour; all profiles have the same scale (see Fig. 9B and Fig. 11). (B) Stereophotogrammetrically derived topographic profile (Profile 5–11; see Fig. 8 for location) across the volcano from west to east. Triangle indicates basal scarp, note relative elevations of surrounding plains on both sides of the volcano.

assume that the thickness of the fan is on the order of 50–250 m, based on the observation that the fan drapes the basal scarp (which our shadow measurements and stereogrammetric data indicate is of the order of 500 m) and yet is thin enough that the scarp morphology is still detectable. If the deposits were significantly thicker than 250 m, it is unlikely that any expression of the underlying scarp would be detected in the image and topographic data. We measured the fan area to be ~19,100 km^2, so that the fan volume estimate falls within the range 995 to

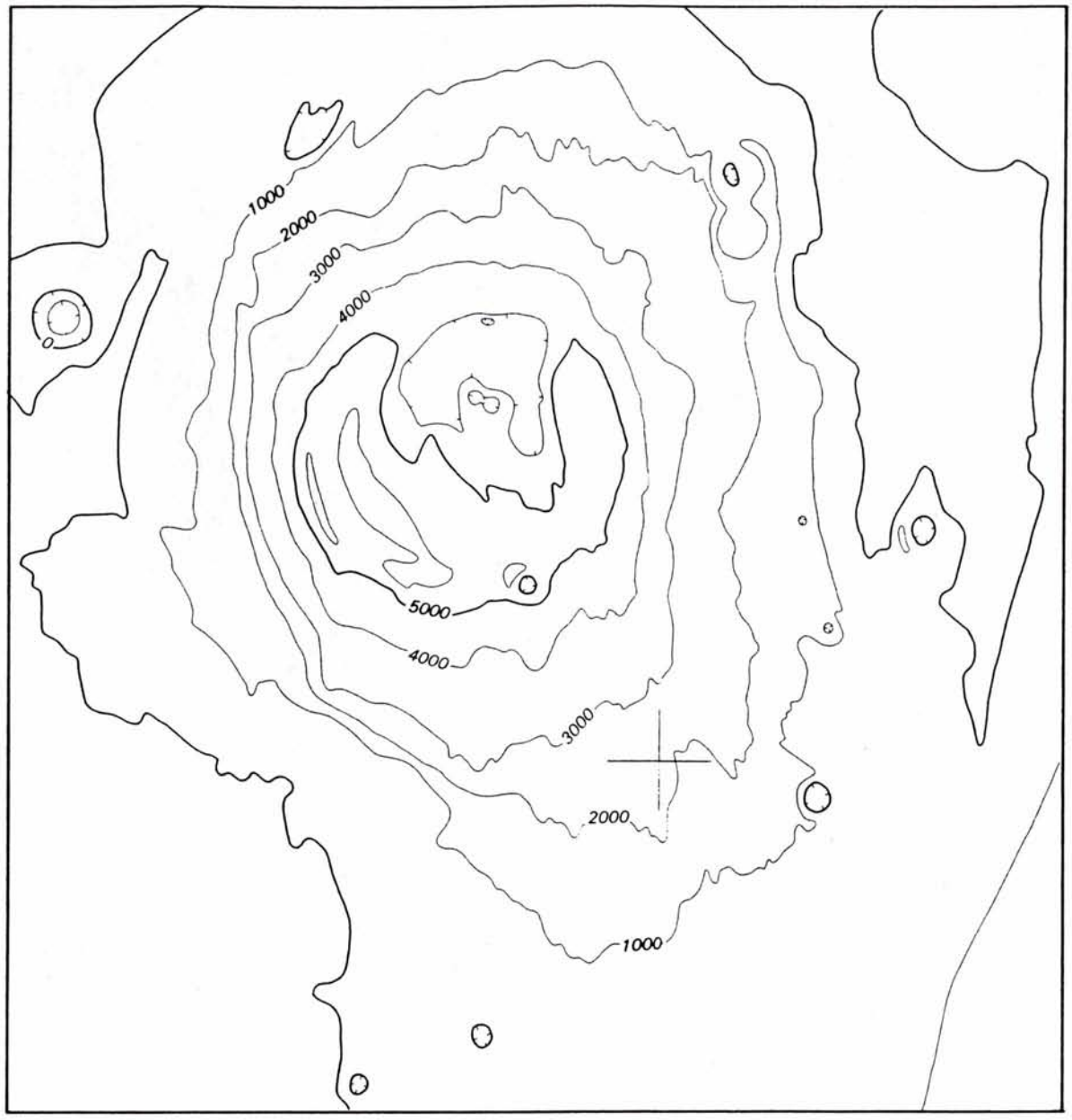

FIG. 10. Topographic map for Apollinaris Patera that was generated in this analysis from stereophotogrammetry. Area of map is matched to that of Fig. 2; contour interval is 1000 m (see also U.S. Geological Survey 1991); total width of map is ~235 km.

4975 km^3, respectively (average ~3000 km^3). We note that Scott and Dohm (in press) mapped the fan deposits as being more extensive to the west; however, including this additional area would not substantially change our volume calculation for the fan. Subtracting our estimate of the fan volume from that of the total volume of Apollinaris Patera results in an estimated volume for the main edifice of 97,000 km^3; the fan deposit comprises only ~3% of the total volume of the volcano. For comparison, the volumes of terrestrial and martian volcanic deposits are listed in Table II.

DISCUSSION

From our morphologic observations, the inferred physical properties of the surface units, and the topographic data, we find that the fan material (f) is significantly different from the main edifice (m). The exact composition of the erupted products that formed Apollinaris Patera is not known. However, a large body of evidence has limited the range of composition of martian volcanic materials to mafic lavas, most likely basalt (c.f. McSween 1985; Banin *et al.* 1992; Soderblom 1992). Thus the range of

TABLE II
Volumes of Materials Composing Certain Volcanic Features on the Earth and Mars

	Volume (10^5 km^3)
Olympus Mons, Mars[a]	26
Hawaiian-Emperor Chain[b]	10
Deccan Plateau, India[c]	8
Alba Patera, Mars[d]	6
Elysium Flood Basalts, Mars[e]	3
Columbia River Basalts, Washington[c]	2
Hadriaca Patera, Mars[f]	1
Apollinaris Patera, Mars[g]	1
Mauna Loa, Hawaii[c]	½

[a] Wu *et al.* 1984.
[b] Clague and Dalrymple 1987.
[c] Crisp 1984.
[d] Wilson and Mouginis-Mark 1987.
[e] Plescia and Crisp 1991.
[f] Crown and Greeley 1993.
[g] This study.

materials that could form the flanks of any martian volcano is thought to be relatively limited and includes pyroclastic airfall deposits, pyroclastic flows, and lava flows (Mouginis-Mark *et al.*, 1992). Because of the relatively friable nature (slumps, sharply incised valleys), lack of distinct lava flow morphology, and apparent uniform circumferential erosion to form the basal scarp, we infer that the main edifice is composed mostly of either air-fall deposits or pyroclastic flows, as has been proposed for Alba Patera (Wilson and Mouginis-Mark 1987, Mouginis-Mark *et al.* 1988), Tyrrhena Patera (Greeley and Crown 1990) and Hadriaca Patera (Crown and Greeley 1993). These explosive eruptions may have been phreatomagmatic in nature.

Due to the easily eroded nature of the flanks it seems likely that any pyroclastic materials that compose the main edifice (m) are mostly poorly to nonwelded. Base surges could result in the proposed valley formation; both base surges and nonwelded deposits are consistent with an explosive origin having a phreatomagmatic component. This inference is supported by the interpretation that chaotic material formed contemporaneously with the volcano, thus indicating a possible source of water to interact with the ascending magma. Additionally, Apollinaris Patera is situated at the debouchment of the large fretted channel Ma'adim Vallis and is in a local basin; thus it is plausible that a large supply of water, ground or ponded, could have been available. Later, after formation of the basal scarp, this source may have been desiccated or isolated from the erupting magma and thus late stage eruptions that formed the fan were different in eruptive *style*.

Our preferred model for fan (f) formation is that it is predominately the result of effusive activity (in contrast to the main edifice), and these lavas were erupted at a low rate. This model is based on three key observations. First, the distinct narrow valleys incised in the main flanks are not apparent on the fan, evidence that the fan is composed of a material exhibiting physical properties that are different from the main edifice (this is supported by the IRTM and color image data), specifically, a more competent material than the main edifice. Second, high relief flow lobes indicative of a'a flows are not identifiable on the fan. Terrestrial a'a flow units typically exhibit relief on the order of 5–15 m, whereas pahoehoe flow units are typically less than 1 m (MacDonald 1972, p. 69–91). Flows seen at other locations on Mars have reported thicknesses of ~20–60 m (Moore *et al.* 1978); if flows of this thickness occurred on the fan they should be identifiable with the existing image data. Third, the fan spreads out from the breach in the caldera into a large fan; terrestrial pahoehoe flows typically spread out if there are no topographic obstacles whereas a'a flows are typically confined by levees and thus often exhibit relatively long narrow flows.

If such eruptions that formed the fan were comparable to the emplacement of terrestrial pahoehoe flow fields, then an effusion rate of less than 5 m^3 sec^{-1} (1.2×10^{-1} km^3 year^{-1}) is implied (Rowland and Walker 1990), so that in total the fan would have taken ~6400 to 32000 terrestrial years to have formed by *continuous* activity (any periods of repose are not included in this estimate).

Observing that a time interval occurred between the formation of the main edifice and the eruption of the fan is interesting in that it indicates a two-stage (at least) eruptive history for Apollinaris Patera. The fan overlies the scarp; therefore, any period of quiescence was sufficiently long for the scarp to form before eruption of the bulk of the fan materials. The measured relief of this basal scarp, which extends around the entire perimeter of the volcano (except where it is mantled by the fan), is generally 500 m and locally up to 1500 m. It seems likely that formation of this scarp required an extended period of time, whether it was the result of tectonic activity or the removal of material through erosive processes.

Understanding the origin and nature of this circumferential basal scarp is important not only for unraveling the geologic history of Apollinaris Patera but is also potentially useful in giving insight to the climatic conditions during the lifetime of the volcano. Our interpretation that the main edifice is composed of poorly to nonwelded pyroclastic material is *consistent* with an erosional model (of unknown mechanism) for the scarp's origin; fragmental (poorly to nonwelded) pyroclastic deposits would be more easily eroded and removed than welded or effusive deposits (Fisher and Schmincke 1976, p. 196). These inferences have implications not only for the formation of the Apolli-

naris Patera basal escarpment, but possibly for the similar feature that surrounds Olympus Mons, particularly in support of an origin by erosion (King and Riehle 1974, Head *et al.* 1976, Lopes *et al.* 1980). A similar period of dormancy that included formation of a basal scarp has been proposed for Olympus Mons based on relative cratering ages of units that compose and surround it (Hiller *et al.* 1982). Olympus Mons' basal scarp is also circumferential though it exhibits much greater relief, >5 km. Parker *et al.* (1989) and Baker *et al.* (1991) have recently proposed that transient shallow seas may have existed on Mars, perhaps in Lower Amazonian times (Baker *et al.* 1991). This time period is compatible with the age of Apollinaris Patera that was determined by crater counts (Plescia and Saunders 1979) and possibly also with the formation of the basal scarp at Olympus Mons (Hiller *et al.* 1982). Previous models for formation of the Olympus Mons basal escarpment have included the erosion of an unconsolidated basal layer of ash or fragmental materials (King and Riehle 1974, Head *et al.* 1976), but each model has been criticized on the basis of its inability to explain the removal of significant volumes of material without the same process affecting the adjacent landscape (Hodges and Moore 1979). If shallow seas were responsible for the erosion of these basal escarpments, then the removal of material from low elevations might be easier to explain. One other martian volcano located on or near a proposed martian sea (see below), Hecates Tholus, has a basal elevation (~1 km) comparable to that of either Olympus Mons or Apollinaris Patera and this third volcano lacks a basal scarp; however, late stage activity at Hecates Tholus (and possibly other martian volcanoes) could have buried any preexisting basal scarps. This "wave erosion model" for the formation of the escarpments around the base of Apollinaris Patera and Olympus Mons remains highly speculative at this point; however, we consider it to be a viable hypothesis assuming the recent evidence presented for the existence of standing bodies of water in the martian lowlands can be substantiated (Baker *et al.* 1991).

The volume of the main edifice is estimated to be $\sim 10^5$ km^3 from our topographic data. Typical effusion rates of terrestrial basaltic eruptions are generally in the range 10^{-2} to 10^{-1} km^3 year^{-1} (Crisp 1984), so a plausible duration of activity, excluding periods of repose, is 10^6 to 10^7 years. To constrain further this estimate it is assumed that, to a first order, the rate of eruption at Apollinaris Patera is similar to that of the Hawaiian Hot Spot. The oldest seamount in the Hawaiian–Emperor chain has an age of 65×10^6 years and the total volume of the chain is estimated to be 10^6 km^3 (Clague and Dalrymple 1987). Therefore, the average rate of eruption for the Hawaiian–Emperor Chain is 1.5×10^{-2} km^3 year^{-1} (including periods of repose). This Hawaiian–Emperor rate must be considered a lower limit due to removal of an unknown amount of material by erosion. If indeed the rate of eruption at Apollinaris Patera is analogous to the Hawaiian Hot Spot, then an estimate of 10^7 years is reasonable for the active lifetime of Apollinaris Patera.

Estimates of volcanic modification of the martian atmosphere can also be made from the topographic data and the inferred eruption rate. Assuming a density of 2000 kg m^{-3}, which is reasonable for analogous terrestrial deposits (basaltic materials), the total mass of erupted material is 2×10^{17} kg. Thus a total mass of 2×10^{15} kg is predicted for the water vapor released into the atmosphere if we assume a value of 1 wt% (Greeley 1987, McSween and Harvey 1993) for the released water content of the parent magma. This estimate may be substantially low due to the input of nonjuvenile water resulting from the interaction of groundwater/ice during phreatomagmatic eruptions. In addition, the fan material would have released $\sim 10^{14}$ kg of water vapor into the martian atmosphere assuming 1 wt% as the water content of its primary melt. Taking our eruption duration estimates and our calculated volume we propose that approximately 10^8 kg year^{-1} (assuming 1 wt%) water vapor was added to the martian atmosphere; for comparison the current total martian atmospheric water budget is estimated to be about 10^{12} kg (Jakosky and Farmer 1982). Released water may have spent a certain period at the surface as liquid depending on existing pressure–temperature conditions. In addition to water, other gases such as CO_2, and SO_2, and aerosols would also be added to the atmosphere. These additional volatiles may have had an even greater modifying effect on the atmosphere than water vapor (Postawko *et al.* 1988). A detailed investigation of these effects is beyond the scope of this paper; however, recent work has indicated that such volcanic outgassing could have had a dramatic effect on both the short and long term climatic evolution of Mars (Wilson and Mouginis-Mark 1987, Postawko *et al.* 1988, Plescia and Crisp 1991).

This study has raised many questions concerning martian volcanism that we hope to test with the rich data that soon will be returned by the Mars Observer (MO) spacecraft. Specifically, the high resolution images returned by the Mars Observer Camera (Malin *et al.* 1992) will allow for the identification of volcanic features down to a resolution of >2 m/pixel. Such data will be particularly useful for identifying lava flow types, such as a'a and pahoehoe and for evaluation of the origin of proposed pyroclastic deposits and the flank valleys. It would be advantageous to inspect the contacts between the volcanic materials, both the fan (f) and the main edifice (m), with the chaotic material (cht) to confirm our interpretations. Other instruments on the MO will have capabilities of deriving compositional data (Christensen *et al* 1992; Boynton *et al.* 1992) which may be able to distinguish the chemical evolution of erupted materials from a martian

volcano. It is conceivable that considerable magmatic variation could occur at a single volcanic edifice such as Apollinaris Patera based on our estimate of an active lifetime $>10^7$ years. We consider Apollinaris Patera to be a prime target for data acquisition during the Mars Observer Mission.

CONCLUSIONS

Our analyses of the geology, physical properties, and topography of Apollinaris Patera lead us to the following conclusions about the volcano.

(1) On the basis of new topographic data and an estimated rate of eruption of 1.5×10^{-2} km^3 year^{-1}, including periods of repose, we conclude that the volcano was active over an extended period of martian geologic time. Initially, the main edifice (m) was formed over a period of $\sim 10^7$ years, and then the volcano experienced a period of quiescence during which the basal scarp formed and the valleys were incised in the main flanks (duration unconstrained). Next, activity at the summit formed the present large outer caldera and floor materials (cf1). After, or during late stages of outer caldera (cf1) activity, the materials that formed the fan were erupted over $\sim 10^4$ years. Finally, after emplacement of the fan materials (f) the smaller, inner caldera and associated floor materials (cf2) formed over an unconstrained time period.

(2) Morphologic analysis suggests that a significant portion of the main edifice (m) is composed of poorly to nonwelded pyroclastic deposits (as opposed to effusive materials), possibly including a phreatomagmatic component.

(3) It seems likely that the fan material on the southern flank of Apollinaris Patera was formed by low effusion rate eruptions comparable to the formation of a terrestrial compound pahoehoe lava flow field. If correct, this is the first time that such activity has been identified as an integral part of the evolution of a martian shield volcano and thus constrains the eruption rate of the fan materials to $\sim 10^{-1}$ km^3 year^{-1}.

(4) Chaotic material (cht) was formed during the active lifetime of the volcano and may be the result of a volcanically modified geothermal gradient.

(5) The well-constrained topography of the volcano permits an accurate estimate to be made for its volume: $\sim 10^5$ km^3. Combining these new topographic data and assuming reasonable values for the bulk density of the main edifice (~ 2.0–2.5×10^3 kg m^{-3}) and the released water from the magma (1 wt%), then at least 2×10^{15} kg of water was added to the martian atmosphere as a consequence of these eruptions. This is a lower estimate as it does not include any water vapor that may have been generated by phreatomagmatic activity.

APPENDIX: STEREOPHOTOGRAMMETRIC PROFILES

This appendix presents the remainder of new topographic data for Apollinaris Patera (see Fig. 11) as well as a summary of our analysis of the precision of these data. We refer the reader to Fig. 8 for locations of the profiles presented in Fig. 11. As a check on the precision of the derived stereophotogrammetric data, we selected our profiles to maximize the number of intersections in order to examine the repeatability of the measurements. The average repeatability was 305 m with a standard deviation of 234 m for 20 intersections (Table III). Thus we report the precision of these data to be ~300 m. Some profile locations coincide with shadow measurements from the higher resolution, low sun images (accuracy ~100 m; see Fig. 3). In all cases the two data sets are consistent within the precision of the stereophotogrammetry (300 m). This good agreement with the shadow measurements indicates that the profile data may have an accuracy as high as 300 m: this accuracy is internal to the stereo model, accuracy relative to the Mars datum is not quantifiable by this method.

TABLE III
Listing of Intersections of Stereophotogrammetric Profiles

Int	Profile	Avg	Profile	Avg	Diff
1	p1-8	1703	p2-13	1990	287
2	p1-8	4900	p3-10	448	413
3	p1-8	4900	p12-4	4393	507
4	p1-8	4247	p11-5	3940	307
5	p1-8	4360	p2-9	4383	23
6	p1-8	3917	p13-7	3797	120
7	p1-8	4100	p12-6	3917	183
8	p10-3	4290	p12-6	4470	180
9	p10-3	4073	p13-7	3467	606
10	p10-3	4417	p12-4	4330	87
11	p10-3	5010	p2-9	6033	1023
12	p11-5	243	p6-12	-63	306
13	p11-5	4130	p10-3	4030	100
14	p11-5	4163	p13-7	4010	153
15	p11-5	4130	p2-9	4393	263
16	p12-4	4940	p13-7	5203	263
17	p12-4	4590	p2-9	5147	557
18	p12-6	4353	p2-9	4103	250
19	p12-6	5777	p7-13	5863	86
20	p13-7	3467	p2-9	3860	393

Note. Column 1 (Int) is the number assigned to a particular intersection, columns 2 and 4 list intersecting profiles (see Fig. 8 for locations) while columns 3 and 5 show their respective elevations (average of three samples closest to intersection). The last column represents the absolute value of the difference between the two columns. The actual collection of data along the profile from the stereoplotter is a function of time. The data collection does not occur at a consistent speed, thus distances between samples are not consistent nor are the data collected continuously; gaps exist between actual data points. In most cases no common points exist between intersecting profiles. Therefore, we took an average of the three points nearest the intersection and used this in our comparison. High frequency topography could cause an apparent "glitch" in a calculated intersection difference. For example, intersection 11 has the largest difference; we note that the intersection occurs over a ridge on the summit plateau that runs subparallel to one of the profiles. Thus, some of the offset between profiles could reflect actual topographic undulations on the surface (see Figs. 9 and 11 for plots of these topographic data).

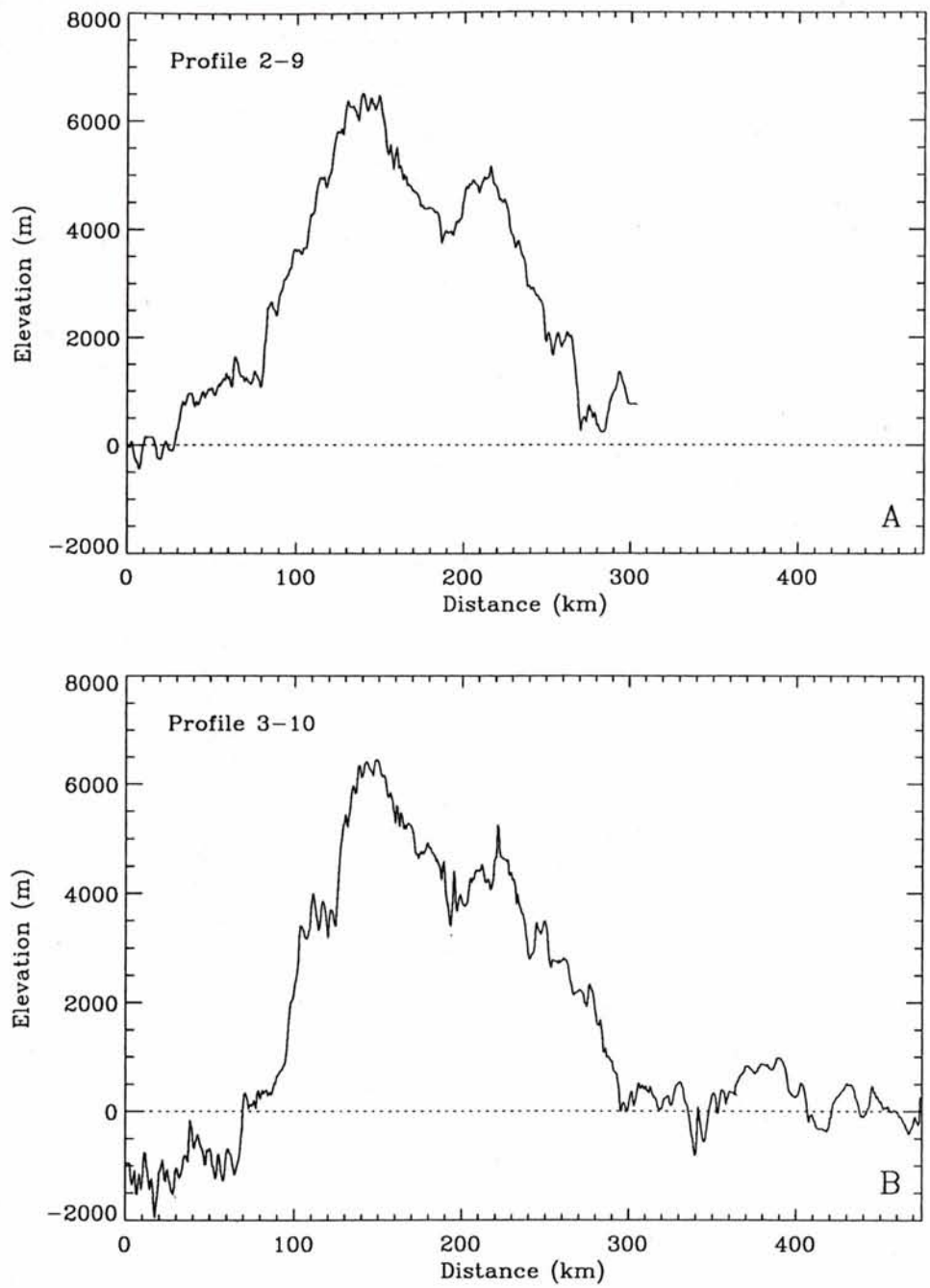

FIG. 11. (A–F) Stereophotogrammetrically derived topographic profiles across Apollinaris Patera (see Fig. 8 for locations). The dotted line indicates the zero elevation for reference, all profiles have the same scale (see also Fig. 9).

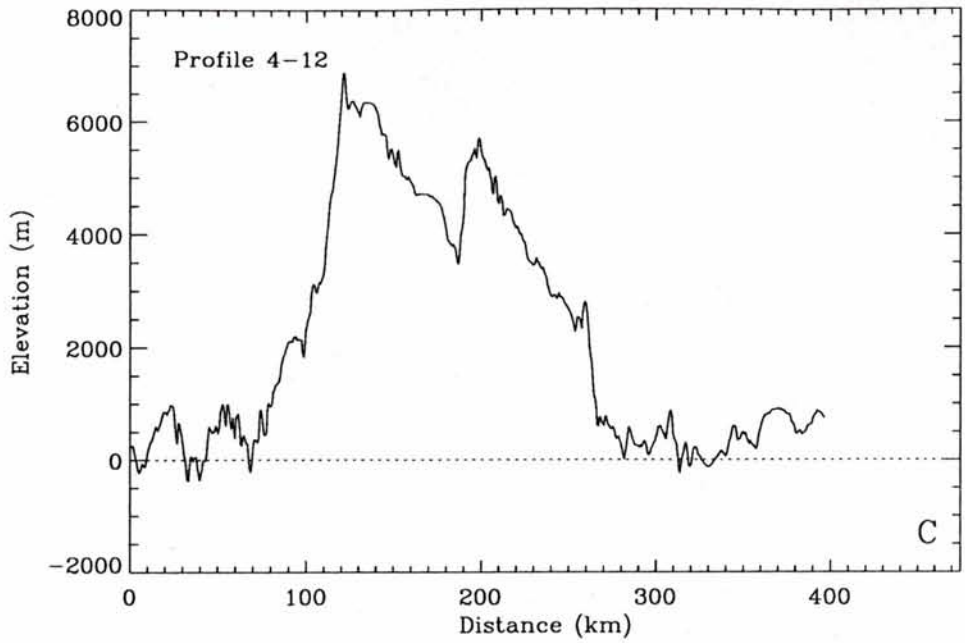

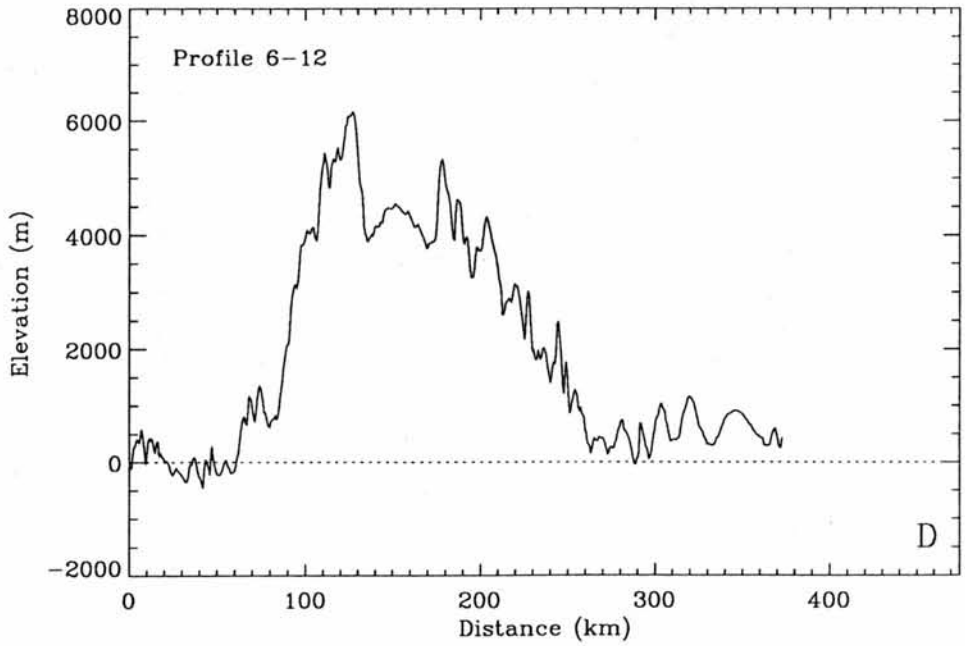

FIG. 11–*Continued*

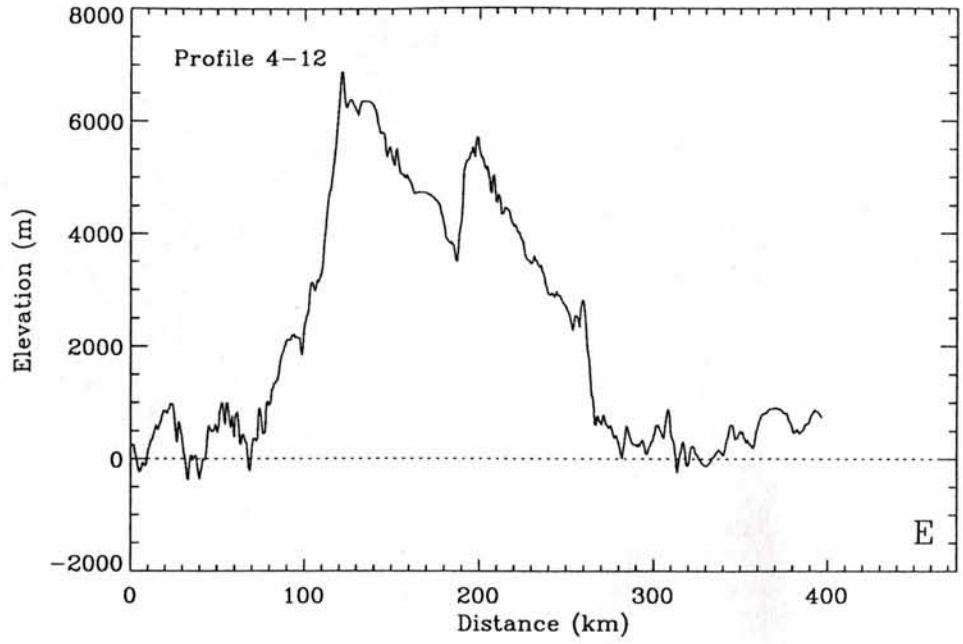

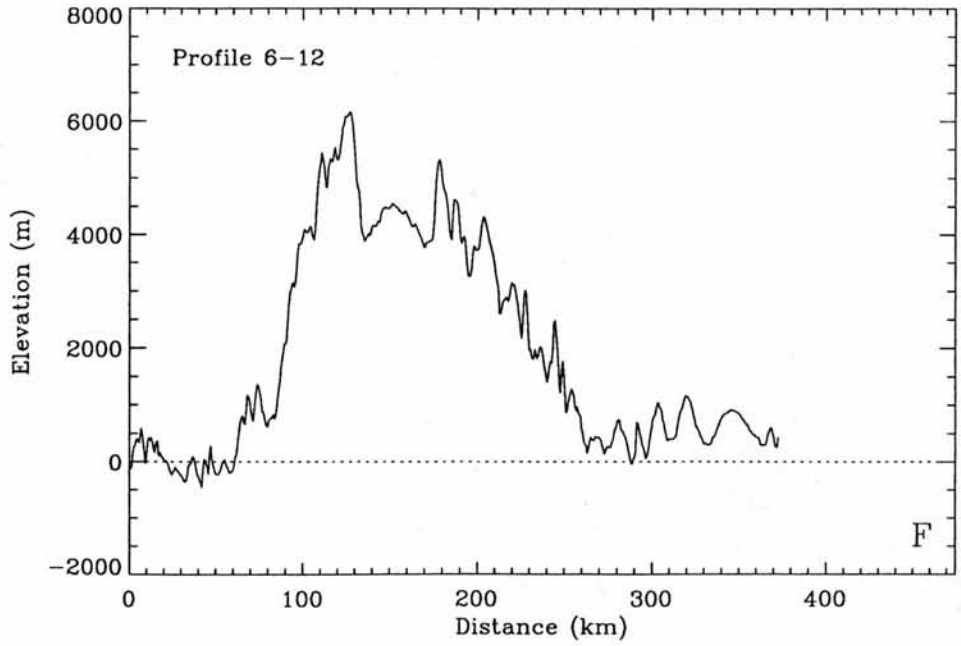

FIG. 11–*Continued*

ACKNOWLEDGMENTS

M.S.R. and P.M-M. were supported by Grant NAGW-437 from NASA's Planetary Geology and Geophysics Program. Portions of this work were also supported by a Smithsonian Institution Graduate Fellowship (M.S.R.). Helpful discussions with S. Rowland and B. Clark are most appreciated (both University of Hawaii). R. Craddock (Smithsonian Institution), K. Tanaka, D. Scott, and J. Dohm (U.S. Geological Survey) provided very helpful reviews on an early version of this paper. Thanks to V. Baker (University of Arizona) for reviewing the manuscript and D. Crown (JPL) for reviewing the manuscript and providing helpful discussions. The U.S. Geological Survey, Flagstaff, Arizona, provided the Planetary Image and Cartography System (PICS), which was essential to several aspects of this study. This is Planetary Geosciences Paper No. 728 and SOEST Contribution No. 3219.

REFERENCES

ARTHUR, D. W. G. 1977. Limitations of the narrow angle convergent pair. *Photogramm. Eng. Remote Sens.* **43,** 1511–1514.

ARTHUR, D. W. G. 1978. Precise Mars relative altitudes. In *National Aeronautics and Space Administration Technical Memorandum 80339,* p. 397.

ARVIDSON, R. E., E. A. GUINESS, M. A. DALE-BANNISTER, J. ADAMS, M. SMITH, CHRISTENSEN, AND R. B. SINGER 1989. *J. Geophys. Res.* **94,** 1573-1587.

BAKER, V. R. 1982. *The Channels of Mars.* Univ. of Texas Press, Austin.

BAKER, V. R., R. G. STROM, V. C. GULICK, J. S. KARGEL, G. KOMATSU, AND V. S. KALE 1991. Ancient oceans, ice, sheets, and the hydrological cycle of Mars. *Nature* **352,** 589–594.

BANIN, A., B. C. CLARK, AND H. WANKE 1992. Surface Chemistry and Mineralogy. In *Mars* (H. H. Kieffer, B. M. Jakosky, C. W. Snyder, and M. S. Mathews, Eds.), pp. 594–625. Univ. of Arizona Press, Tucson.

Basaltic Volcanism Study Project 1981. *Basaltic Volcanism on the Terrestrial Planets.* Pergamon, New York.

BLASIUS, K. R., AND J. A. CUTTS 1981. Topography of martian central volcanoes. *Icarus* **45,** 87–112.

BLOOM, A. L. 1978. *Geomorphology.* Prentice–Hall, Englewood Cliffs, NJ.

BOYNTON, W. V., J. I. TROMBKA, W. C. FELDMAN, J. R. ARNOLD, P. A. J. ENGLERT, A.E. METZGER, R. C. REEDY, S. W. SQUYRES, H. WANKE, S. H. BAILEY, J. BRUCKNER, J. L. CALLAS, D. M. DRAKE, P. DUKE, L. G. EVANS, E. L. HAINES, F. C. MCCLOSKEY, H. MILLS, C. SHINOHARA, AND R. STARR 1992. Science applications of the Mars Observer Gamma Ray Spectrometer. *J. Geophys. Res.* **97,** 7681–7698.

CARR, M. H. 1981. *The Surface of Mars.* Yale Univ. Press, New Haven, CT.

CARR, M. H., AND G. G. SCHABER 1977. Martian permafrost features. *J. Geophys. Res.* **82,** 4039–4054.

CARR, M. H., AND R. GREELEY 1980. *Volcanic features of Hawaii; A Basis of Comparison with Mars.* NASA SP-403.

CHRISTENSEN, P. R., AND R. W. ZUREK 1984. Martian north polar hazes and surface ice: Results from the Viking Survey/Completion mission. *J. Geophys. Res.* **89,** 4587–4596.

CHRISTENSEN, P. R., D. L. ANDERSON, S. C. CHASE, R. N. CLARK, H. H. KEIFFER, M. C. MALIN, J. C. PEARL, J. CARPENTER, N. BANDIERA, F. G. BROWN, AND S. SILVERMAN 1992. Thermal Emission Spectrometer experiment: Mars Observer Mission. *J. Geophys. Res.* **97,** 7719–7734.

CLAGUE, D. A. AND G. B. DALRYMPLE 1987. *The Hawaiian–Emperor Volcanic Chain.* U.S. Geological Professional Paper 1350, Vol. 1, pp. 5–54.

CRISP, J. A. 1984. Rates of magma emplacement and volcanic output. *J. Volcanol. Geotherm. Res.* **20,** 177–211.

CROWN, D. A., L. A. LESHIN, AND R. GREELEY 1988. *IRTM Analysis of Possible Explosive Volcanic Deposits on Mars.* NASA TM-4041, pp. 349–351.

CROWN, D. A., AND R. GREELEY 1993. The volcanic geology of Hadriaca Patera and the eastern Hellas region of Mars. *J. Geophys. Res.* **98,** 3431–3451.

FISHER, R. V. 1977. Erosion by volcanic base-surge density currents: U-shaped channels. *Geol. Soc. Am. Bull.* **88,** 1287–1297.

FISHER, R. V, AND H.-U. SCHMINKE *Pyroclastic Rocks,* Springer-Verlag, New York.

GREELEY, R. 1987. Release of juvenile water on Mars: Estimated amounts and timing associated with volcanism. *Science* **236,** 1653—1654.

GREELEY, R. AND P. D. SPUDIS 1981. Volcanism on Mars. *Revs. Geophys. Space Phys.* **19,** 13–41.

GREELEY, R., AND J. E. GUEST 1987. *Geologic Map of the Eastern Equatorial Region of Mars.* U.S. Geological Survey Miscellaneous Investigations Series Map I-1802-B.

GREELEY, R., AND D. A. CROWN 1990. Volcanic geology of Tyrrhena Patera, Mars. *J. Geophys. Res.* **95,** 7133–7149.

GULICK, V. C., AND V. R. BAKER 1990. Origin and evolution of valleys on martian volcanoes. *J. Geophys. Res.,* **95,** 14325–14344.

HARMON, J. K., M. P. SULZER, P. J. PERILLAT, AND J. F. CHANDLER 1992. Mars Radar Mapping: Strong backscatter from the Elysium Basin and outflow channel. *Icarus* **95,** 153–156.

HEAD, J. W., M. SETTLE, AND C. A. WOOD 1976. Origin of Olympus Mons escarpment by erosion of pre-volcano substrate. *Nature* **263,** 667–668.

HERKENHOFF, K. E., AND B. C. MURRAY, 1990. Color and albedo of the south polar layered deposits on Mars. *J. Geophys. Res.* **95,** 1343–1358.

HILLER, K. H., P. JANLE, G. P. O. NEUKEM, J. E. GUEST, AND R. M. C. LOPES 1982. Mars: Stratigraphy and gravimetry of Olympus Mons and its aureole. *J. Geophys. Res.* **87,** 9905–9915.

HODGES, C. A., AND H. J. MOORE 1979. The subglacial birth of Olympus Mons and its aureoles. *J. Geophys. Res.* **84,** 8061–8074.

JAKOSKY, B. M. AND C. B. FARMER 1982. The seasonal and global behavior of water vapor in the Mars atmosphere: Complete global results of the Viking atmospheric water detector experiment. *J. Geophys. Res.* **87,** 2999–3019.

KIEFFER, H. H., T. Z. MARTIN, A. R. PETERFREUND, B. M. JAKOSKY, E. D. MINER, AND F. D. PALLUCONI 1977. Thermal and albedo mapping of Mars during the Viking primary mission. *J. Geophys. Res.* **82,** 4249–4291.

KIEFFER, H. H., P. A. DAVIS, AND L. A. SODERBLOM 1981. Mars global properties: Maps and applications. *Proc. Lunar Planet. Sci. Conf. 12th,* 1395–1417.

KING, J. S., AND J. R. RIEHLE 1974. A proposed origin of the Olympus Mons escarpment. *Icarus* **23,** 300–317.

LOPES, R. M. C., J. E. GUEST, AND C. J. WILSON 1980. Origin of the Olympus Mons aureole and perimeter scarp. *Moon Planet.* **22,** 221–234.

MACDONALD, G. A. 1972. *Volcanoes.* Prentice–Hall, Englewood Cliffs, NJ.

MALIN, M. C., G. E. DANIELSON, A. P. INGERSOLL, H. MASURSKY, J. VEVERKA, M. A. RAVINE, AND T. A. SOULANILLE 1992. Mars Observer Camera. *J. Geophys. Res.* **97,** 7699–7718.

MCSWEEN, H. Y. 1985. SNC meteorites: Clues to Martian petrologic evolution. *Rev. Geophys.* **23,** 391–416.

MCSWEEN, H. Y. AND R. P. HARVEY 1993. Outgassed water on Mars: Constraints from melt inclusions in SNC meteorites. *Science* **259,** 1890–1892.

MOORE, H. J., D. W. G. ARTHUR, AND G. G. SCHABER 1978. Yield strengths of flows on the Earth, Mars and Moon. *Proc. Lunar Planet. Sci. Conf. 9th,* 3351–3378.

MOUGINIS-MARK, P. J. 1981. Late-stage summit activity of Martian shield volcanoes. *Proc. Lunar Planet. Sci. Conf. 12th,* 1431–1447.

MOUGINIS-MARK, P. J., AND M. S. ROBINSON 1992. Evolution of the Olympus Mons caldera, Mars. *Bull. Volcanol.* **54,** 347–360.

MOUGINIS-MARK, P. J., L. WILSON, AND J. W. HEAD 1982. Explosive volcanism on Hecates Tholus, Mars: Investigation of eruptive conditions. *J. Geophys. Res.* **87,** 9890–9904.

MOUGINIS-MARK, P. J., L. WILSON, AND J. R. ZIMBELMAN 1988. Polygenic eruptions on Alba Patera, Mars. *Bull. Volcanol.* **50,** 361–379.

MOUGINIS-MARK, P. J., L. WILSON, AND M. T. ZUBER 1992. The physical volcanology of Mars. In *Mars* (H. H. Kieffer, B. M. Jakosky, C. W. Snyder, and M. S. Mathews, Eds.), pp. 424–452. Univ. of Arizona Press, Tucson.

NEUKUM, G., AND D. U. WISE 1976. Mars: A standard crater curve and possible new time scale. *Science* **194,** 1381–1387.

NEUKUM, G., AND K. HILLER 1981. Martian ages. *J. Geophys. Res.* **86,** 3097–3121.

PARKER, T. J., R. S. SAUNDERS, AND D. M. SCHNEEBERGER 1989. Transitional morphology in West Deuteronilus Mensae, Mars: Implications for modification of the lowland/upland boundary. *Icarus* **82,** 111–145.

PLESCIA, J. B. 1990. Recent flood lavas in the Elysium region of Mars. *Icarus* **88,** 465–490.

PLESCIA, J. B., AND R. S. SAUNDERS 1979. The chronology of the Martian volcanoes. *Proc. Lunar Planet. Sci. Conf., 10th,* 2841–2859.

PLESCIA, J. B., AND J. CRISP 1991. *Recent Elysium Volcanism—Effects on the Martian Atmosphere.* LPI Technical Report 92-02, pp. 115–116.

POSTAWKO, S. E., F. P. FANALE, AND A. P. ZENT 1988. Effects of epochal vs episodic release of SO_2 by volcanoes on Mars. *Lunar Planet. Sci. Conf. XIX,* 943–944. [Abstract]

REIMERS, C. E., AND P. D. KOMAR 1979. Evidence for explosive density currents on certain martian volcanoes. *Icarus* **39,** 88–110.

ROBINSON, M. S., AND K. L. TANAKA 1990. Magnitude of a catastrophic flood event at Kasei Valles, Mars. *Geology* **18,** 902–905.

ROWLAND, S. K., AND G. P. L. WALKER 1990. Pahoehoe and a'a in Hawaii: Volumetric flow rate controls the lava structure. *Bull. Volcanol.* **52,** 615–628.

SCOTT, D. H., AND J. M. DOHM *Geologic Map of Apollinaris Patera Region of Mars.* U.S. Geological Survey Miscellaneous Investigations Series Map I-2351, in press.

SCOTT, D. H., E. C. MORRIS, AND M. N. WEST 1978. *Geologic Map of the Aeolis Quadrangle of Mars.,* 1:5,000,000. U.S. Geologic Survey Map I-1111.

SHARP, R. P. 1973. Mars: Fretted and chaotic terrains. *J. Geophys. Res.* **78,** 4073–4083.

SODERBLOM, L. A. 1992. The composition and mineralogy of the Martian surface from spectroscopic observations: 0.3 μm to 50 μm. In *Mars* (H. H. Kieffer, B. M. Jakosky, C. W. Snyder, and M. S. Mathews, Eds.), pp. 594–625. Univ. of Arizona Press, Tucson.

SODERBLOM, L. A., C. D. CONDIT, R. A. WEST, B. M. HERMAN, AND T. J. KRIEDLER 1974. Martian planetwide crater distributions: Implications for geologic history and surface processes. *Icarus* **22,** 239–263.

TANAKA, K. L. 1986. The stratigraphy of Mars. *J. Geophys. Res.* **91,** E139–E158.

U.S. Geological Survey 1989. *Topographic Map of Western Equatorial Region of Mars.* U.S. Geological Survey Miscellaneous Investigations Series Map I-2030.

U.S. Geological Survey 1990. *Planetary Image Cartography System Users Manual.*

U.S. Geological Survey 1991. *Topographic Map of the Aeolis Northeast Quadrangle.* U.S. Geological Survey Miscellaneous Investigations Series Map I-2118.

WEST, M. 1974. Martian volcanism: Additional observations and evidence for pyroclastic activity. *Icarus* **21,** 1–11.

WILSON, L., P. J. AND MOUGINIS-MARK 1987. Volcanic input into the atmosphere from Alba Patera on Mars. *Nature* **330,** 354–357.

WU, S. S. C., A. A. ELASSEL, R. JORDAN, AND F. J. SCHAFER 1982. Photogrammetric application of Viking orbital photography. *Planet. Space Sci.* **30,** 45–55.

WU, S. S. C., P. A. GARCIA, R. JORDAN, F. J. SCHAFER, AND B. A. SKIFF 1984. Topography of the shield volcano, Olympus Mons on Mars. *Nature* **309,** 432–435.

WU, S. S. C., R. JORDAN, AND F. J. SCHAFER 1985. *Compilation of 1:2,000,000-Scale Topographic Map Series.* NASA Technical Memorandum 87563, pp. 612–613.

WU, S. S. C., R. JORDAN, AND F. J. SCHAFER 1988. *Progress in Compilation of 1:2,000,000-Scale Topographic Map Series:* NASA Technical Memorandum 4041, p. 553.

ZIMBELMAN, J. R. 1984. *Geologic Interpretation of Remote Sensing Data for the Martian Volcano Ascraeus Mons,* NASA Technical Memorandum 88784, pp. 271–572.

ZIMBELMAN, J. R., AND H. H. KIEFFER 1979. Thermal mapping of the northern equatorial and temperate latitudes of Mars. *J. Geophys. Res.* **84,** 8239–8251.

ZIMBELMAN, J. R., AND R. GREELEY 1983. Elevation-dependent corrections for thermal inertias on Mars. *Lunar Planet. Sci. Conf. XIV,* 879–880. [Abstract]

ZIMBELMAN, J. R., AND L. A. LESHIN 1987. A geologic evaluation of thermal properties for the Elysium and Aeolis quadrangles of Mars. *J. Geophys. Res.* **92,** E588–596.

ZIMBELMAN, J. R., AND K. S. EDGETT 1992. The Tharsis Montes, Mars: Comparison of volcanic and modified landforms. *Proc. Lunar Planet. Sci. Conf. 22nd,* 31–44.